Naval Research Laboratory
Washington, DC 20375-5000

DTIC FILE COPY

NRL Memorandum Report 6055

AD-A187 085

Bubble Dynamics in a Turbulent Ship Wake

M. B. STEWART AND E. W. MINER

Laboratory for Computational Physics and Fluid Dynamics

November 5, 1987

DTIC
ELECTE
DEC 2 1 1987
S D
H

87 12 4 023

Approved for public release, distribution unlimited

SECURITY CLASSIFICATION OF THIS PAGE

REPORT DOCUMENTATION PAGE

1a. REPORT SECURITY CLASSIFICATION UNCLASSIFIED	1b RESTRICTIVE MARKINGS AD-A187085
2a. SECURITY CLASSIFICATION AUTHORITY	3 DISTRIBUTION / AVAILABILITY OF REPORT Approved for public release; distribution unlimited.
2b DECLASSIFICATION / DOWNGRADING SCHEDULE	
4. PERFORMING ORGANIZATION REPORT NUMBER(S) NRL Memorandum Report 6055	5 MONITORING ORGANIZATION REPORT NUMBER(S)
6a. NAME OF PERFORMING ORGANIZATION Naval Research Laboratory 6b. OFFICE SYMBOL (If applicable)	7a NAME OF MONITORING ORGANIZATION Office of the Chief of Naval Research
6c. ADDRESS (City, State, and ZIP Code) Washington, DC 20375-5000	7b. ADDRESS (City, State, and ZIP Code) Arlington, VA 22217
8a. NAME OF FUNDING / SPONSORING ORGANIZATION Office of the Chief of Naval Research 8b OFFICE SYMBOL (If applicable)	9 PROCUREMENT INSTRUMENT IDENTIFICATION NUMBER
8c. ADDRESS (City, State, and ZIP Code) Arlington, VA 22217	10. SOURCE OF FUNDING NUMBERS PROGRAM ELEMENT NO: 62111N; PROJECT NO: RU11W 71-801; TASK NO:; WORK UNIT ACCESSION NO: DN156-264

11 TITLE (Include Security Classification)
Bubble Dynamics in a Turbulent Ship Wake

12. PERSONAL AUTHOR(S)
Stewart, M.B. and Miner, E.W.

13a. TYPE OF REPORT	13b TIME COVERED	14 DATE OF REPORT (Year, Month, Day)	15 PAGE COUNT
Interim	FROM 1/1/87 TO present	1987 November 5	48

16 SUPPLEMENTARY NOTATION

17 COSATI CODES			18 SUBJECT TERMS (Continue on reverse if necessary and identify by block number)
FIELD	GROUP	SUB-GROUP	Bubble Ship wake Finite volume Turbulence

19 ABSTRACT (Continue on reverse if necessary and identify by block number)

A numerical model of the dynamics of the bubble distribution in a ship's wake is described. This wake is initiated by air entrained by the bow wave, the bilges, and the propeller. The present model is a finite volume formulation of the parabolic Navier-Stokes equations describing the hydrodynamic wake and the Garrettson equations describing bubble transport. The model is used to simulate the hydrodynamic and bubble wake found behind a twin screw ship 100 meters long. Both the initial hydrodynamic wake and bubble conditions were generated using empirical techniques. The model was used to predict bubble profiles for a range of bubble radius. In addition, a sensitivity analysis was used to determine the relative importance of each of the terms in the bubble transport equations. The dynamics of larger bubbles were dominated by the relat vely large rise velocities and turbulent diffusion. The dynamics of the smaller bubbles were dominated by turbulent diffusion and the bubble loss from gas diffusion.

20 DISTRIBUTION / AVAILABILITY OF ABSTRACT X UNCLASSIFIED/UNLIMITED ☐ SAME AS RPT ☐ DTIC USERS	21 ABSTRACT SECURITY CLASSIFICATION UNCLASSIFIED
22a NAME OF RESPONSIBLE INDIVIDUAL Michael B. Stewart	22b TELEPHONE (Include Area Code) (202) 767-2858 22c OFFICE SYMBOL Code 4430

DD FORM 1473, 84 MAR 83 APR edition may be used until exhausted
All other editions are obsolete

SECURITY CLASSIFICATION OF THIS PAGE

☆U.S. Government Printing Office. 1985—607-

CONTENTS

Accession For
NTIS GRA&I ☑
DTIC TAB ☐
Unannounced ☐
Justification
By
Distribution/
Availability Codes
Dist | Avail and/or Special
A-1

Bubble Dynamics in a Turbulent Ship Wake

Introduction

Bubbles found in the upper ocean are interesting for a number of reasons. The acoustical properties of ship wakes using active sonar are largely determined by the concentration and distribution of bubbles (Schmidt, 1972). This property has been known and used since WW II. In the study of oceanography, near surface gas bubbles are important in underwater sound propagation (Shulkin 1968,1969), meteorology (Blanchard and Woodcock 1957), sea surface chemistry (Sutcliffe, Baylor and Menzel 1963), cavitation (Fox and Herzfeld 1959), and air-sea gas exchange (Kanwisher 1963). In-situ measurements of near surface bubble populations typically exploit the fact that at bubble resonance frequency, the absorption and scattering cross section of the bubbles can be 1000 times its geometrical cross section (Medwin 1970). Recently, photographic procedures have also been used (Johnson and Cooke 1979, and Bezzabotnov 1985) to measure near-surface bubble populations. Optical methods have also been used by Ling and Pao (1987) to measure bubble distributions.

Theoretical investigations into the dynamics of bubble motion were first begun using a Boltzmann-type transport equation in 7 dimensional space (Garrettson 1973). Several solutions were generated for greatly simplified situations using the method of characteristics. This method essentially transforms the equations from an Eulerian reference frame to Lagrangian and then separates it into manageable pieces. This procedure was possible only because the equations were first order and quasi-linear. Another formulation of the equations governing bubble dynamics (Smith, Hyman and Uzes 1986) use a subset of Garrettsons equations but add an empirical diffusive flux similar to equations describing sediment driven flows. The addition of the diffusion term makes the equations second order and eliminates the use of the method of characteristics. The equations were cast into a parabolic form and were solved with the parabolic Navier-Stokes equations for a ships wake.

An entirely Lagrangian approach has also been used (Miner, Griffin and Skop 1986). These equations were solved for the case of bubbles rising through a quiescent fluid experiencing volume changes by gas diffusion and hydrostatic pressure variations. Finally, the equations governing bubble motion have been solved exactly in the zero Reynolds number limit (Stewart and Morrison 1981). In general, the exact solution usually remains in Fourier transformed space but may be inverted in closed form to real space for several special cases including air bubbles in water. All cases can be inverted numerically. In theory this result is completely general for any bubble rising through a moving fluid, however, bubble volume changes due to gas diffusion and hydrostatic pressure variations are ignored. The importance of this work is the prediction of bubble resonance in an acoustical field for particular frequencies and it gives some indication

Manuscript approved May 31, 1987.

of the size of the turbulent diffusive flux term found in the equations solved by Smith et. al. (1986).

Procedure

Hydrodynamic Variables

The turbulent wake extending behind a ship is distinguished from the ambient ocean by the 3 mean flow velocities (U, V, and W), 6 Reynolds stresses ($u'u'$, $v'v'$, $w'w'$, $u'v'$, $u'w'$, $v'w'$), the thermal scar, and the white water wake. In this model we follow the practice of the previous investigators (Garrettson 1973, Smith et. al. 1986, and Miner et.al. 1986) and solve the hydrodynamic variables (mean velocities and Reynolds stresses) with only one-way coupling to the bubble field. Thermal wakes have been treated previously (Stewart 1987). If the void fraction of entrained air is sufficiently small, the effect of the bubbles on the hydrodynamic variables will be negligible. For cases where this coupling may be important, it can be included relatively easily using the PSI-cell method (Crowe 1978). In the fully parabolic region away from the ship and the free surface, the void fraction should be small enough that one-way coupling is justified in the modeling.

The parabolic form of the Navier-Stokes equations are shown in Table 1. The Reynolds stresses are calculated from values of the turbulent kinetic energy/dissipation. The form used is an anisotropic extension of the usual isotropic equations (Baker 1982). The equations governing turbulent kinetic energy, turbulent dissipation, and the Reynolds stresses are also found in Table 1.

Initial Conditions

The initial conditions for the hydrodynamic variables were based on a superposition of wake and jet correlations for simplified geometrical shapes to produce an approximate ships wake. The basic ship used was the DE 1006 with length 94 m., beam 11 m., and draft 3.7 m. The initial axial and transverse velocity components are shown in Figures 1 a,b. The primary vortex shown in this profile is caused by the propeller. In real ship wakes, the bilge vortex, propeller vortex, and bow wave vortex usually combine to produce something considerably more complex, sometimes with multiple vorticies. At this time, there is no satisfactory method for supplying initial conditions either with experimental measurements or accurate estimates. This subject is currently being investigated.

The calculations for the hydrodynamic variables were made extending 3 km. behind the ship. The decay of the axial and transverse velocity components is shown in figures 1.

Table 1 Parabolic Navier-Stokes Equations and Reynold Stress

Momentum:

$$\frac{\partial(\rho u^2)}{\partial x} + \frac{\partial(\rho vu)}{\partial y} + \frac{\partial(\rho wu)}{\partial z} = \frac{\partial \tau^t_{u,xz}}{\partial y} + \frac{\partial \tau^t_{u,xy}}{\partial z} - \frac{\partial \overline{P}}{\partial x} + F_x$$

$$\frac{\partial(\rho uv)}{\partial x} + \frac{\partial(\rho v^2)}{\partial y} + \frac{\partial(\rho wv)}{\partial z} = \frac{\partial \tau^t_{v,xz}}{\partial y} + \frac{\partial \tau^t_{v,xy}}{\partial z} - \frac{\partial \overline{P}}{\partial y} + F_y$$

$$\frac{\partial(\rho uw)}{\partial x} + \frac{\partial(\rho vw)}{\partial y} + \frac{\partial(\rho w^2)}{\partial z} = \frac{\partial \tau^t_{w,xz}}{\partial y} + \frac{\partial \tau^t_{w,xy}}{\partial z} - \frac{\partial \overline{P}}{\partial z} + F_z$$

Continuity:

$$\frac{\partial(\rho u)}{\partial x} + \frac{\partial(\rho v)}{\partial y} + \frac{\partial(\rho w)}{\partial z}$$

Where

τ^t is the total Reynolds and molecular stress
$\frac{\partial P}{\partial x}$ is known prior to the calculation
P(x,y) is adjusted to satisfy continuity
u,x act in the axial or streamwise direction
v,y act in the horizontal, transverse coordinate direction
w,z act in the vertical, transverse coordinate direction
F is the momentum source term

Reynolds Stresses

$$\overline{u'^2} = C_1 k - C_2 C_4 \frac{k^3}{\epsilon^2}((\frac{\partial u}{\partial y})^2 + (\frac{\partial u}{\partial w})^2) - 2C_4 \frac{k^2}{\epsilon}(\frac{\partial u}{\partial x})$$

$$\overline{v'^2} = C_3 k - C_2 C_4 \frac{k^3}{\epsilon^2}(\frac{\partial u}{\partial y})^2 - 2C_4 \frac{k^2}{\epsilon}(\frac{\partial v}{\partial y})$$

$$\overline{w'^2} = C_3 k - C_2 C_4 \frac{k^3}{\epsilon^2}(\frac{\partial u}{\partial z})^2 - 2C_4 \frac{k^2}{\epsilon}(\frac{\partial w}{\partial z})$$

$$\overline{u'v'} = -C_4 \frac{k^2}{\epsilon}\frac{\partial u}{\partial y} - C_2 C_4 \frac{k^3}{\epsilon^2}(\frac{\partial u}{\partial z}(\frac{\partial v}{\partial z} + \frac{\partial w}{\partial y}) + 2\frac{\partial v}{\partial y}(\frac{\partial u}{\partial x} + \frac{\partial v}{\partial y}))$$

$$\overline{u'w'} = -C_4 \frac{k^2}{\epsilon}\frac{\partial u}{\partial z} - C_2 C_4 \frac{k^3}{\epsilon^2}(\frac{\partial u}{\partial y}(\frac{\partial w}{\partial y} + \frac{\partial v}{\partial z}) + 2\frac{\partial w}{\partial z}(\frac{\partial u}{\partial x} + \frac{\partial w}{\partial z}))$$

$$\overline{w'v'} = -C_4 \frac{k^2}{\epsilon}(\frac{\partial v}{\partial z} + \frac{\partial w}{\partial y}) - C_2 C_4 \frac{k^3}{\epsilon^2}(\frac{\partial u}{\partial z}\frac{\partial u}{\partial y})$$

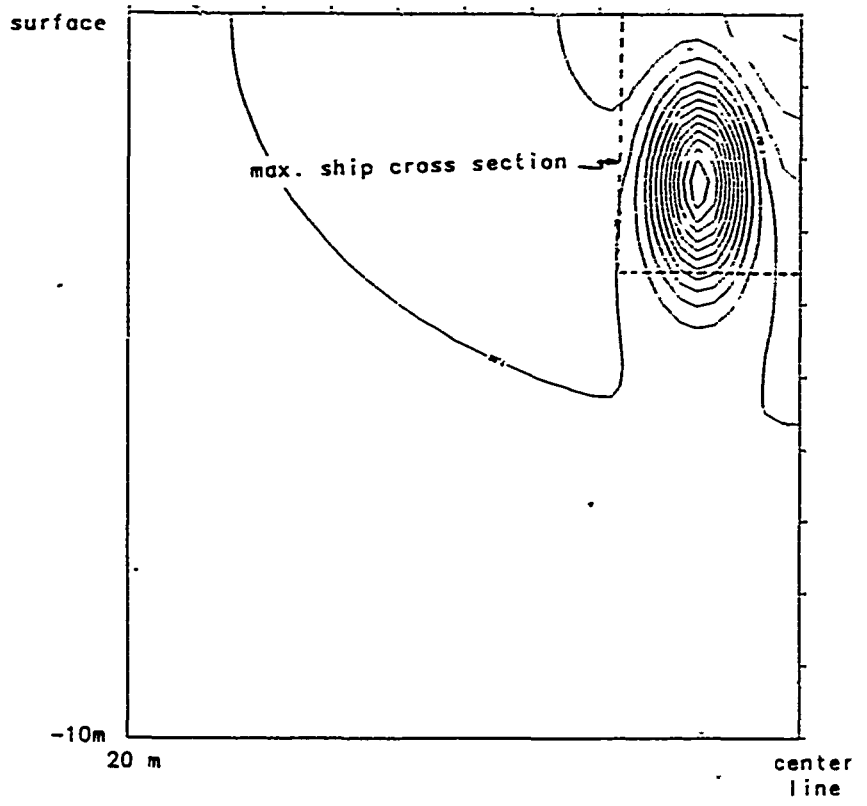

Fig. 1a Initial U (axial) Velocity

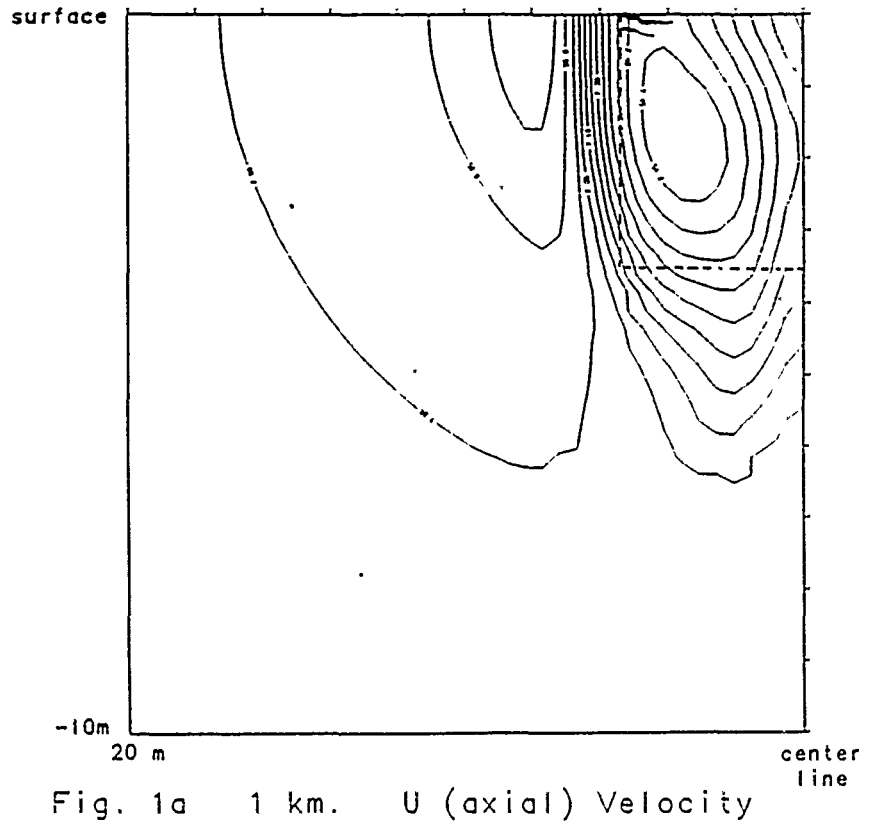

Fig. 1a 1 km. U (axial) Velocity

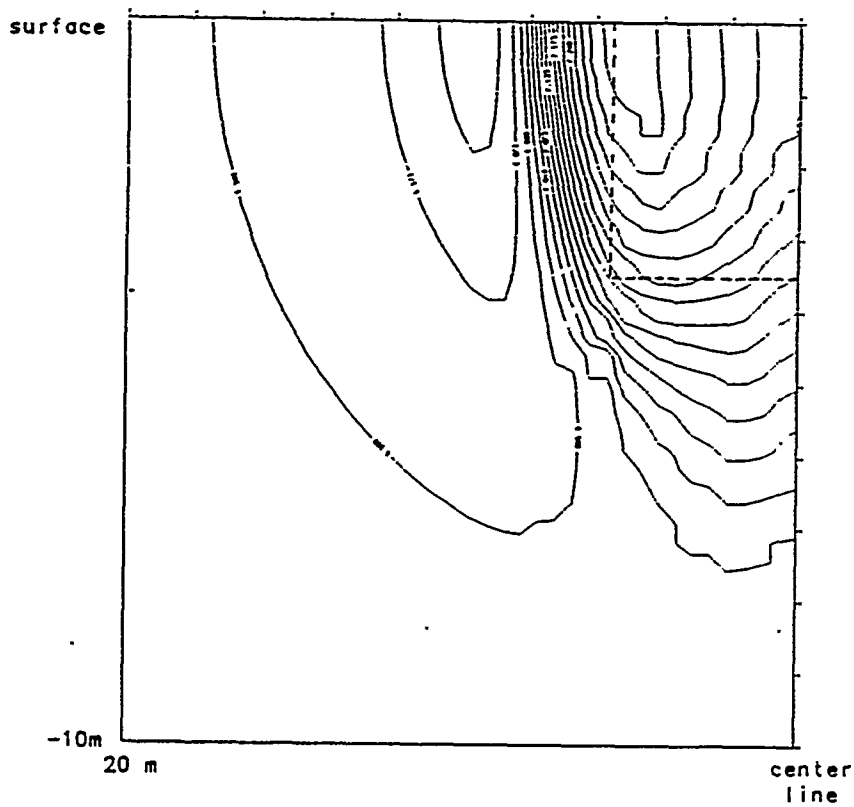

Fig. 1a 2 km. U (axial) Velocity

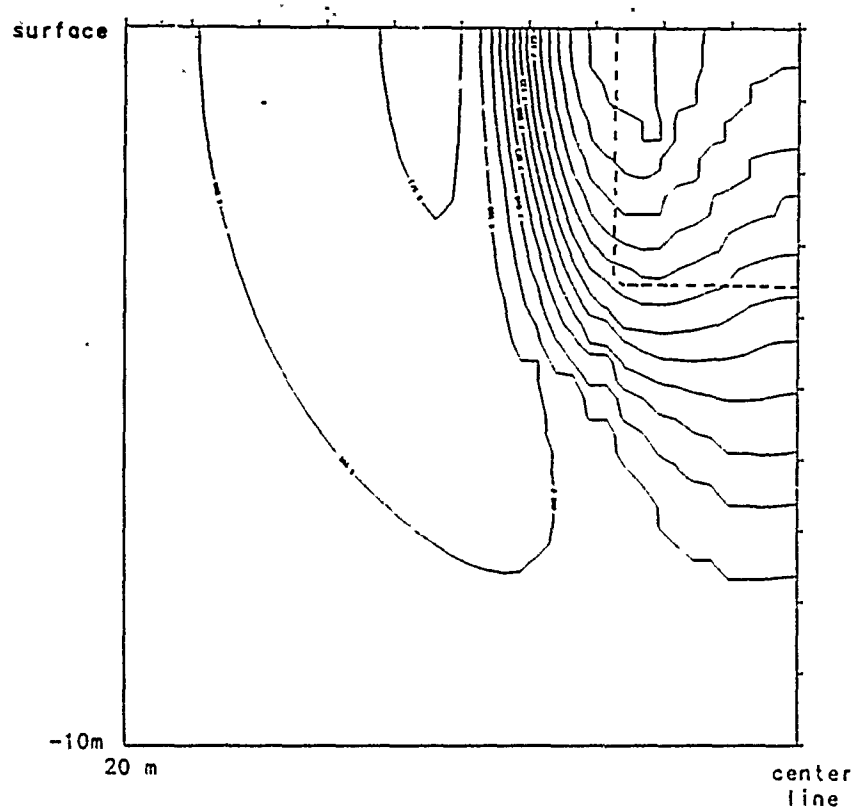

Fig. 1a 3 km. U (axial) Velocity

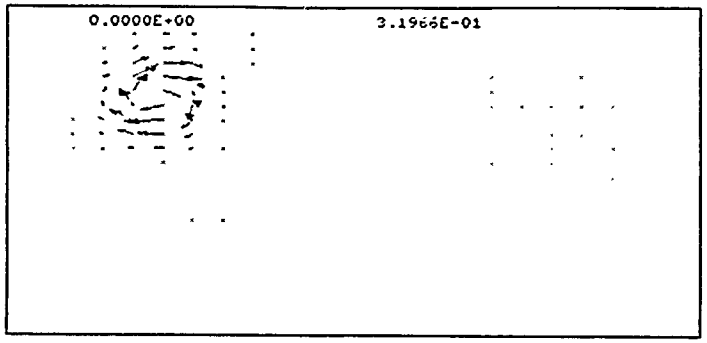

initial conditions

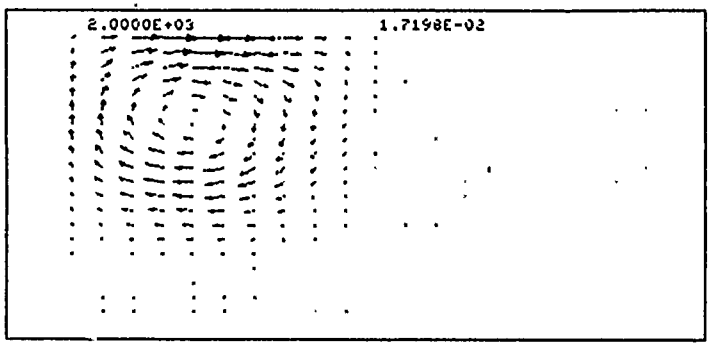

2 km.

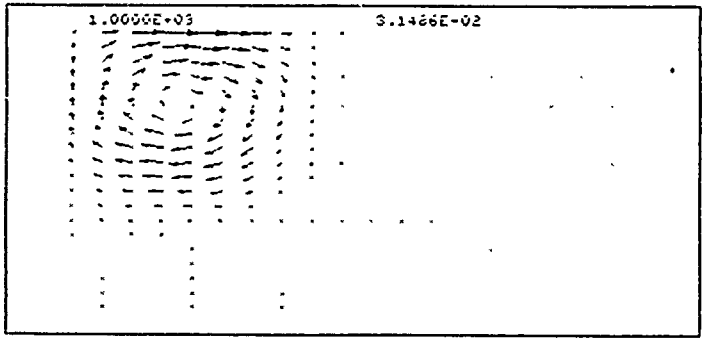

1 km.

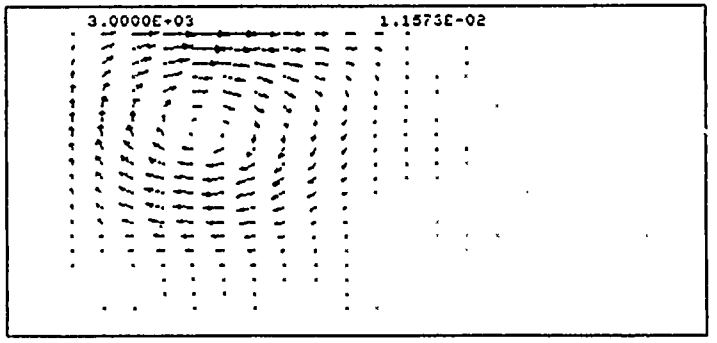

3 km.

Fig. 1b Swirl Velocities

The primary convective influence of the ships velocity field on the bubble distribution are the transverse velocity components. This is because the bubble distribution will have strong gradients in the transverse directions and have only weak gradients in the axial coordinate which is consistent with the parabolic assumption used in all the transport equations.

The initial conditions for the bubble distribution found behind a ship were estimated using the method of Smith et. al. (1986).

Bubble Transport Equations

There are two basic techniques used to model two phase flow. One is the Eulerian-Eulerian approach where both phases are treated as continua. This technique works well in dense flows and where the conveyed phase (bubbles) are continuously distributed throughout the conveying phase (water). It is least effective where the conveyed phase is found only at discreet locations.

The second approach is an Eulerian-Lagrangian approach where the conveying phase is a continuum and the conveyed phase is modeled at discreet locations. Using this approach the hydrodynamic variables would be solved using the usual parabolic form of the Navier-Stokes equations and the bubble equations would be solved using a simultaneous Lagrangian integration of the bubble position, velocity, and radius. Both methods have been used recently to model bubble dynamics in the upper ocean (Garrettson 1973, Smith et. al. 1986 and Miner et. al. 1986).

A conceptual framework which appears to incorporate both techniques is the bubble transport theory (Garrettson 1973). This procedure sums the flux of bubbles in position space, velocity space, and radius space and sets that equal to all other sources of bubbles (i.e. organic decay, cavitation, or electrolysis). After some rearrangement, the bubble transport equation is derived, equation 1, table 2. As shown, equation represents a particularly complex form of the Eulerian approach. Examination of the equation reveals it to be a first order, quasilinear partial differential equation. As such, it can be greatly simplified using the method of characteristics. The result is shown in equations 2, table 2. Here the equations are of the Lagrangian type. The bubble density is integrated from equation 2a simultaneously with equations governing bubble position, velocity, and radius (equations 2b-2d). These equations (2b-2d) require modeling to predict bubble velocity, acceleration, and radius change rate. To some extent, the assumptions and models used are a matter of personal preference. Some representative ones can be found in Clift et. al. 1978.

The approach used here is the Eulerian form of Garrettsons equations. The equations are formed in 7 dimensional space, 3 position coordinates, 3 velocity coordinates, and

Table 2 Bubble Transport Equations

EulerianForm

$$\frac{\partial \Psi}{\partial t} = \overrightarrow{v} \cdot \nabla_r \Psi + \overrightarrow{a} \cdot \nabla_v \Psi + \nu \frac{\partial \Psi}{\partial l} = S - \Sigma_t \Psi, \tag{1}$$

where,

Ψ = Bubble number density $[m^{-3}]$

t = time [s]

$\overrightarrow{v}$ = Bubble velocity $[\frac{m}{s}]$

$\nabla_r = (\frac{\partial}{\partial x}, \frac{\partial}{\partial y}, \frac{\partial}{\partial z})[m^{-1}]$

$\nabla_v = (\frac{\partial}{\partial u}, \frac{\partial}{\partial v}, \frac{\partial}{\partial w})[\frac{s}{m}]$

$\overrightarrow{a}$ = Bubble acceleration $[\frac{m}{s^2}]$

$\nu = \frac{\partial l}{\partial t}[\frac{m}{s}]$

l = Bubble radius [m]

s = sources or sinks

$\Sigma_t = \nabla_v \cdot \overrightarrow{a} + \frac{\partial \nu}{\partial l}$

LagrangianForm

$$\frac{D\Psi}{Dt} = S - \Sigma_t \Psi \tag{2a}$$

$$\frac{D\overrightarrow{r}}{Dt} = \overrightarrow{v} \tag{2b}$$

$$\frac{D\overrightarrow{v}}{Dt} = \overrightarrow{a} \tag{2c}$$

$$\frac{Dl}{Dt} = \nu \tag{2d}$$

1 radius coordinate. If the equations are descretized in all 7 coordinates the computer memory and cpu requirements would be quite large. Instead, a simplification of the equations is made based on estimates of the transient response of a bubble to the ships hydrodynamic wake. The modeling assumptions used here are;

1. Transients involving relative motion between a bubble and the mean velocity of the surrounding fluid are negligible, ie less than 100 micro seconds (Stewart and Morrison 1981). Thus bubble motion is the same as the local water except for a steady state rise velocity which is a function of bubble radius.

2. Steady relative motion between the bubble and the surrounding fluid is best described by a no slip condition at the interface (Clift et. al. 1978).

These assumptions lead to a quasi-steady bubble response in which the bubble velocity is always approximated by the fluid velocity plus steady bubble rise velocity. In this way, all partial derivatives with respect to velocity are zero. Some possible deviations from this behavior will be discussed in a later section.

The effect of bubble radius could not be modeled as simply. As a result, an additional dimension was added to the array containing the bubble number density to reflect the addition of bubble radius as an additional coordinate. The modeling assumption used here was that bubble radius changed with pressure (hydrostatic and surface tension) according to the ideal gas law and with gas diffusion which was proportional to the pressure difference between bubble pressure and water partial pressure (Garrettson 1973).

In addition to the Garrettson equations, another term was added. This term, similar to the one used by Smith et.al. (1986), simulates the effect of turbulent diffusion on bubble position. This approach is commonly used in sedimentation driven flows (see for example Devantier and Larock 1986). In the report by Smith, the the diffusion coefficient was the same as that used in sedimentation driven flows due to the lack of more accurate information.

It is possible to speculate on the value of the turbulent diffusion cofficient. Typically it is set equal to a constant (referred to here as a Prandlt number) times the eddy viscosity. Smith et. al. used a Pr equal to 1. Sedimentation flows are driven by particles whose density are greater than the surrounding fluid. Bubbles, of course, have negligible internal density. Stewart and Morrison (1981) have determined that low density particles respond much more vigorously to a fluctuating fluid velocity than do high density particles. In fact, bubbles can resonate at 3 times the water fluctuation amplitude. A neutrally buoyant particle will follow the water motion, and a heavy particle will move with a smaller amplitude fluctuation. The difference depends on the

frequency with the greatest differences at higher frequencies. Assuming that sediment has a density near that of water, bubbles would respond 3 times more vigorously than sediment at high frequencies.

In addition, there would be a scale effect. Larger bubbles whose diameter is larger than the most energetic turbulent eddies would not be as strongly affected. The influence of several eddies would be integrated over the bubble surface canceling the dispersion effect. For the case of a bubble much larger than the scale of turbulence, the effect is an increase in the drag force between the bubble and the fluid (Stewart and Morrison 1982b) causing the bubble to be more closely entrained.

Thus for a given size bubble, there is an optimum scale of turbulence. This effect could be much greater if the sediment data used in calculating the Prandtl number found in Smith et.al. had a density much greater than the water. Qualitatively this behavior is suggested by the response of bubbles to sonar. Small bubbles resonate at an optimum frequency. The large bubble cut off is calculated by using the bubble diameter which is larger than the maximum wavelength needed for resonance. The smaller bubbles have larger frequency bands during which resonance occurs but the scattering cross section and bubble half life both decrease with decreasing bubble radius.

In this case, space was discretized with a 40 X 40 grid in the transverse plane, the axial coordinate was effectively discretized with 3100 parabolic steps, and bubble radius was discretized using 10 increments. In addition to computer storage, each additional bubble radius increment added another complete equation to solve. The entire set of bubble equations are coupled. Despite being coupled, no iterations were used to produce a completely converged set of bubble equations at each axial location. Instead, the usual parabolic procedure was used where the axial step is kept small enough so that the coupling from the previous step is used in the current step. Table 3 contains the form of the bubble transport equations which were used in this study together with all of the modeling assumptions.

Compared to the code solving only the hydrodynamic equations, this code required more than twice the storage and required the solution of 16 differential equations instead of 6. On a minicomputer, the hydrodynamic code required 10 hours of cpu time. The full bubble wake code required from 37 to 111 hours of cpu time depending on the system usage. When run on the Cray XMP supercomputer execution was completed in 8 minutes of cpu time.

Results

Hydrodynamic Equations

The initial conditions for the fluid velocity components are shown in figures 1. The solution was marched downstream with a variable axial step size based on maximum change of the U velocity component but never exceeding 1 meter. Dependent variables were printed at 1 km., 1.5 km., 2 km., 2.5 km., and 3 km. Figures 1 show the evolution of the flow variables. As expected, the flow velocities gradually die out and the propeller vortex expands. These results are primarily of interest only as input to the evolution of the bubble distribution. The fluid velocity profiles are the same for all computer runs. As stated earlier, the hydrodynamic equations are coupled to the bubble transport equations in one direction only. This can be changed if a situation arises where the bubble number density is large enough to influence the water motion. This one way coupling is justified by the large bubble spacing (void fraction) commonly found in the ocean (Medwin 1970).

Bubble Transport Equations

Full Equations

The first results which will be described are for the full equations. These equations represent the Garrettson bubble transport equations plus turbulent diffusion as implemented by Smith et. al. (1986). The initial conditions and downstream print locations are the same as for the hydrodynamic variables. Although there were 10 discrete bubble radii used from 10 microns to 200 microns, only 5 representative sizes are shown at the 1, 2, and 3 km. stations.

Figures 2-6 show bubble distributions at the various print stations. The behavior appears to be very reasonable. The smaller bubbles have very small terminal rise velocities and are essentially entrained with the propeller vortex and diffused by the turbulence. The smallest bubbles dissolve very rapidly via gas diffusion. The 10 micron bubbles have disappeared before the first print station at 1 km. Although the correlation used to model gas diffusion was determined under 'realistic' conditions (Garrettson 1973), there is some evidence that the estimates are too high (Garrettson 1973 and Miner et. al. 1986). In both cases, predictions showed the smallest bubbles completely dissolving in a very short time. Miner found a very small diffusion rate gave the best agreement with the available data. Garrettson found that eliminating the diffusion of gas from the bubble gave a better fit with experimental data. The reduction in gas diffusion could either be caused by the surfactant cap usually found on bubbles reducing circulation

Table 3 Bubble Equations and Models

$$\vec{v} \cdot \nabla_r \Psi + \nu \frac{\partial \Psi}{\partial l} = S - \Sigma_t \Psi + D \nabla^2 \Psi$$

Models

$D \propto \frac{k^2}{\epsilon}$ - Turbulent Diffusion Coefficient

$\frac{\partial}{\partial v} \equiv 0$ - Bubble velocity is a single valued function of fluid velocity and bubble size

$\Sigma_t = \frac{\partial \nu}{\partial l}$

$\frac{\partial \Psi}{\partial t} = 0$ - parabolic

$n = \frac{\frac{4}{3}\pi l^3 P}{RT}$ - ideal gas in the bubble

$\frac{\partial n}{\partial t} = -GKl^2(P - f)$ Gas diffusion

$P = P_0 - \rho_0 g z + \frac{2\zeta}{l}$ - Bubble pressure

f = partial pressure of the gas in the water

ζ = surface tension of clean water

w = vertical velocity = fluid velocity + rise velocity

$w_{rise} = \frac{F_B}{6\pi\mu l \lambda}$

$\lambda = 1 + .15Re^{.687}$ - finte Reynolds number effect

Re = Reynolds number = $\frac{\rho l w}{\mu}$

u,v = fluid velocity

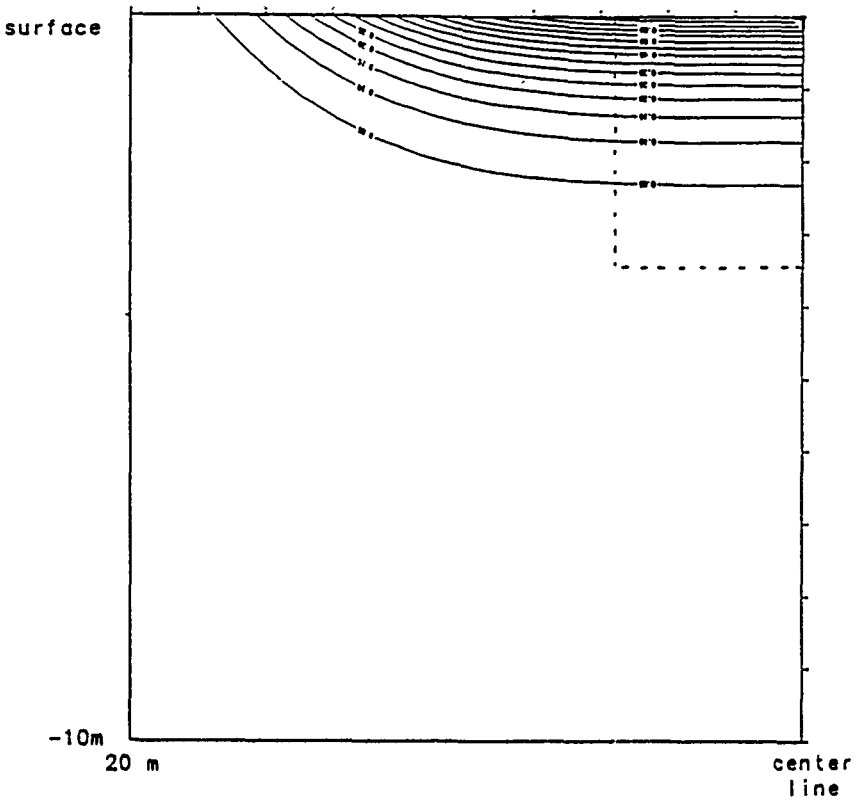

Initial Bubble Distribution

Fig. 2a Full Equations, Pr=.7, 10 microns

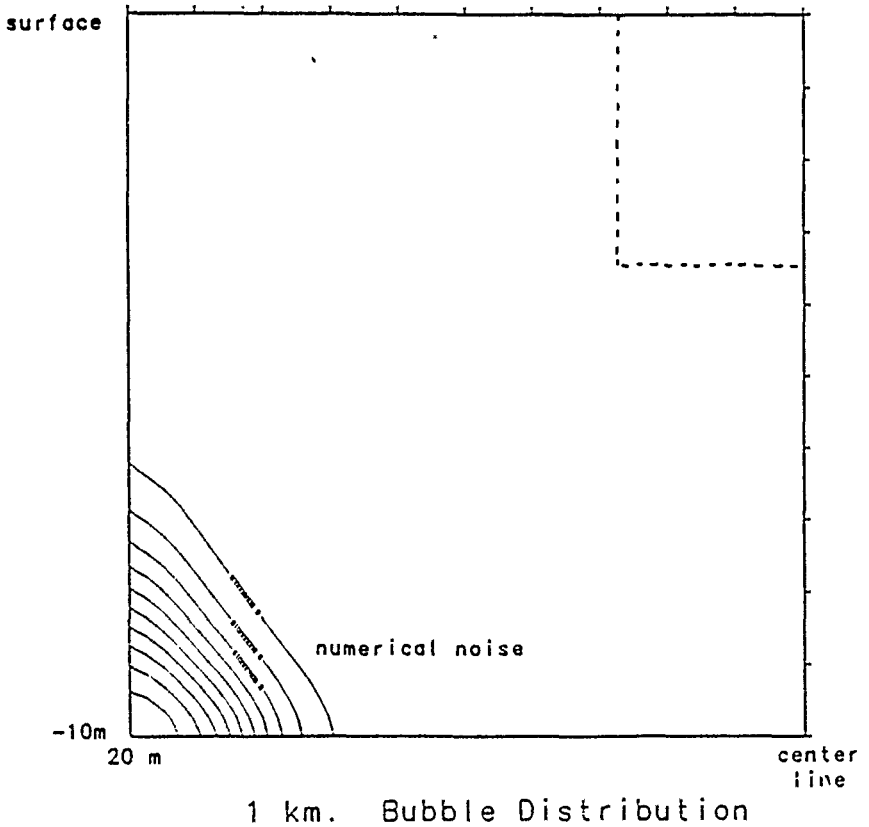

1 km. Bubble Distribution

Fig. 2b Full Equations, Pr=.7, 10 microns

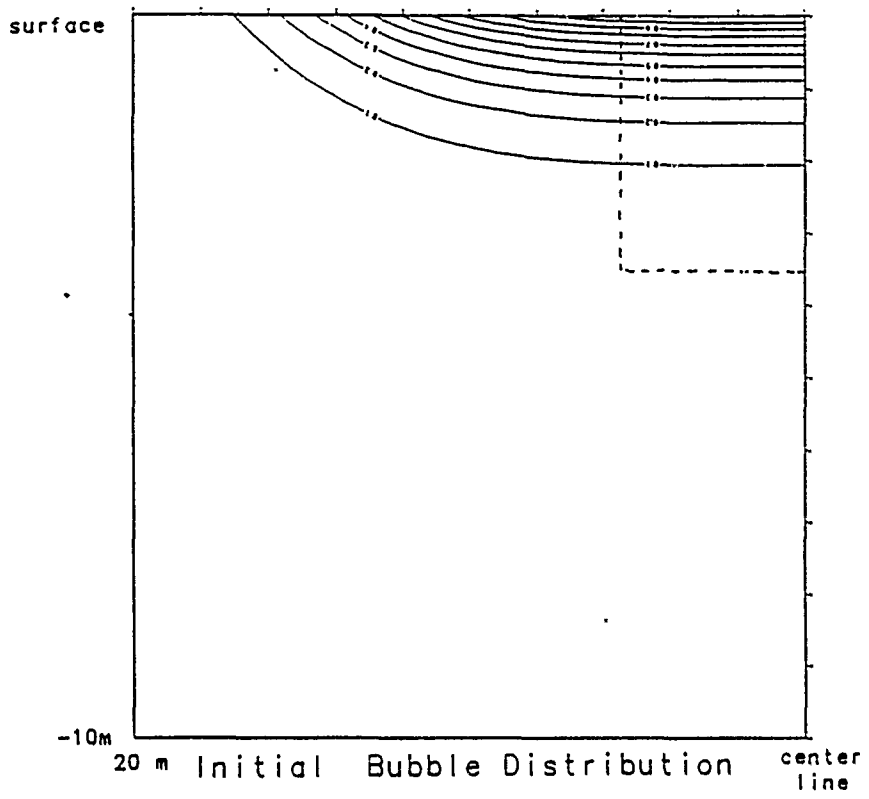

Fig. 3a Full Equations, Pr=.7, 52 microns

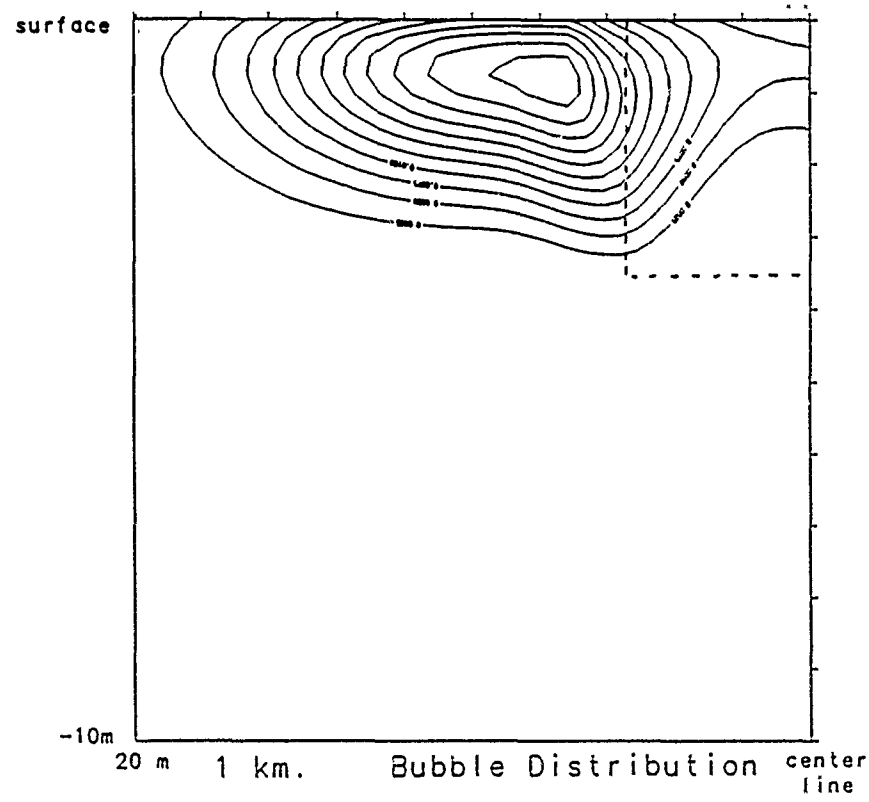

Fig. 3b Full Equations, Pr=.7, 52 microns

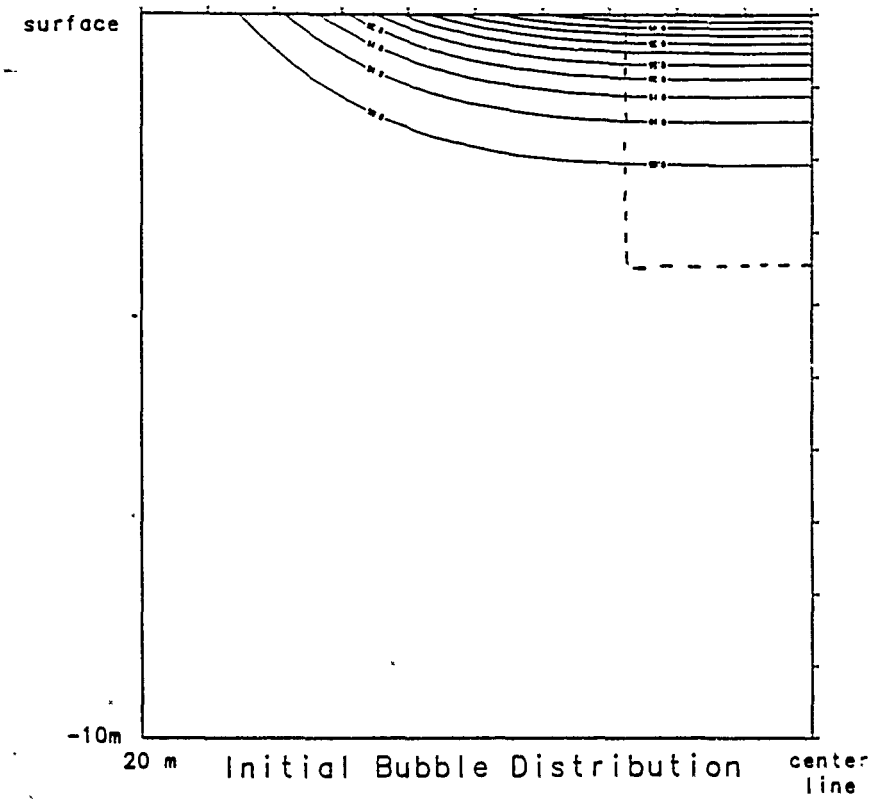

Fig. 4a Full Equations, Pr=.7, 94 microns

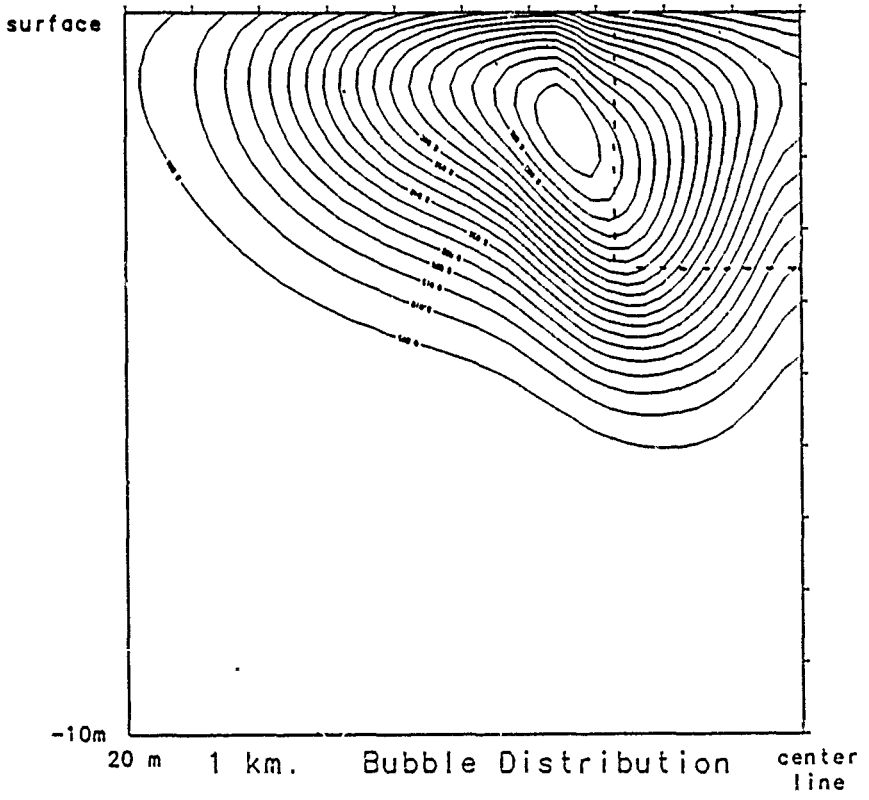

Fig. 4b Full Equations, Pr=.7, 94 microns

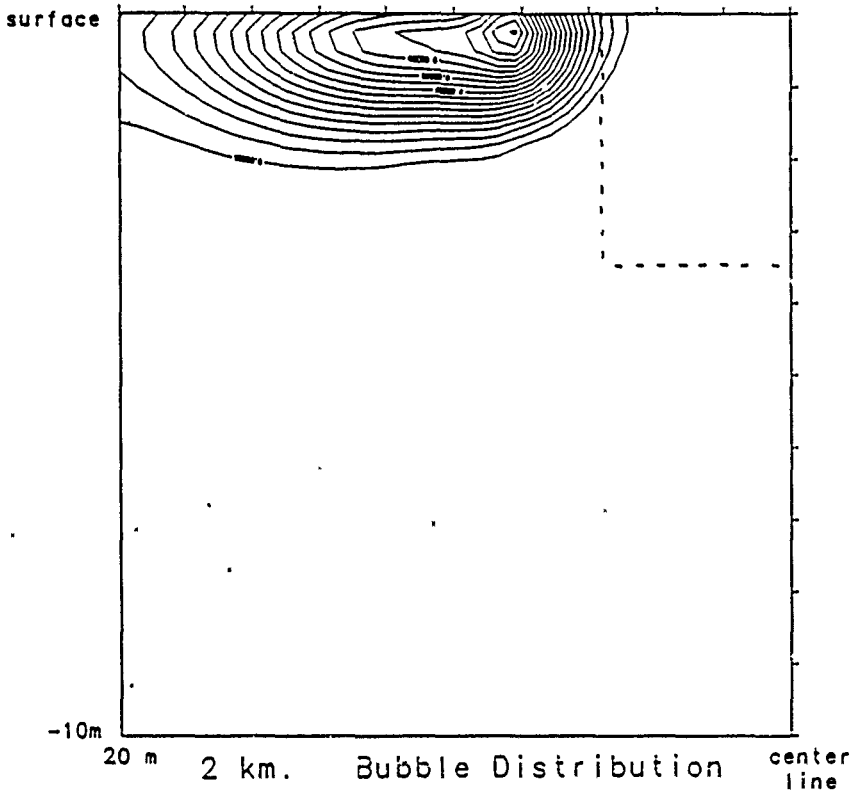

Fig. 4c Full Equations, Pr=.7, 94 microns

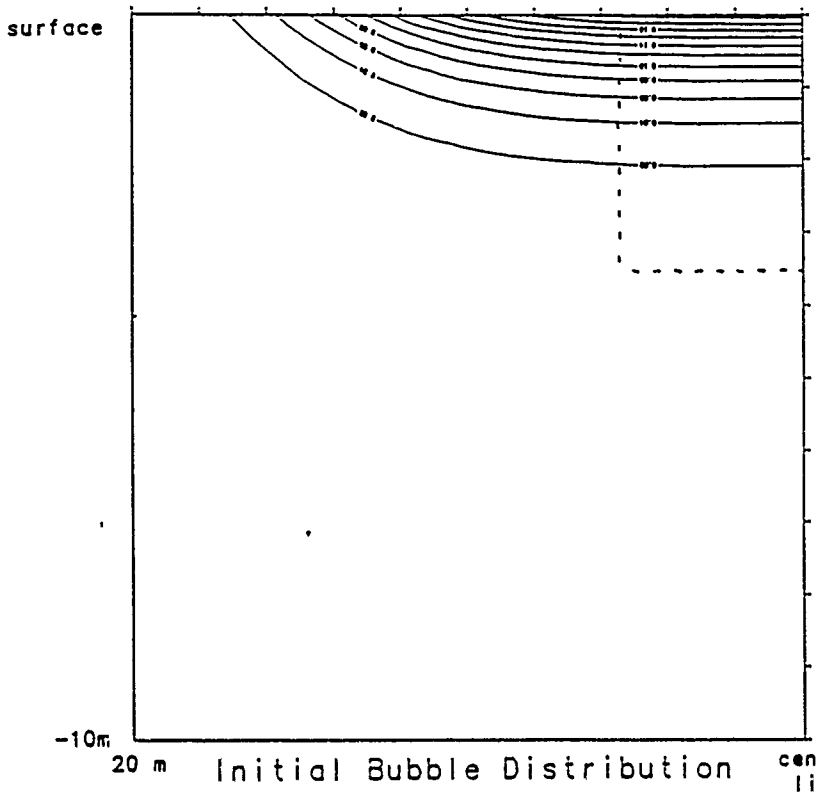

Fig. 5a Full Equations, Pr=.7, 137 microns

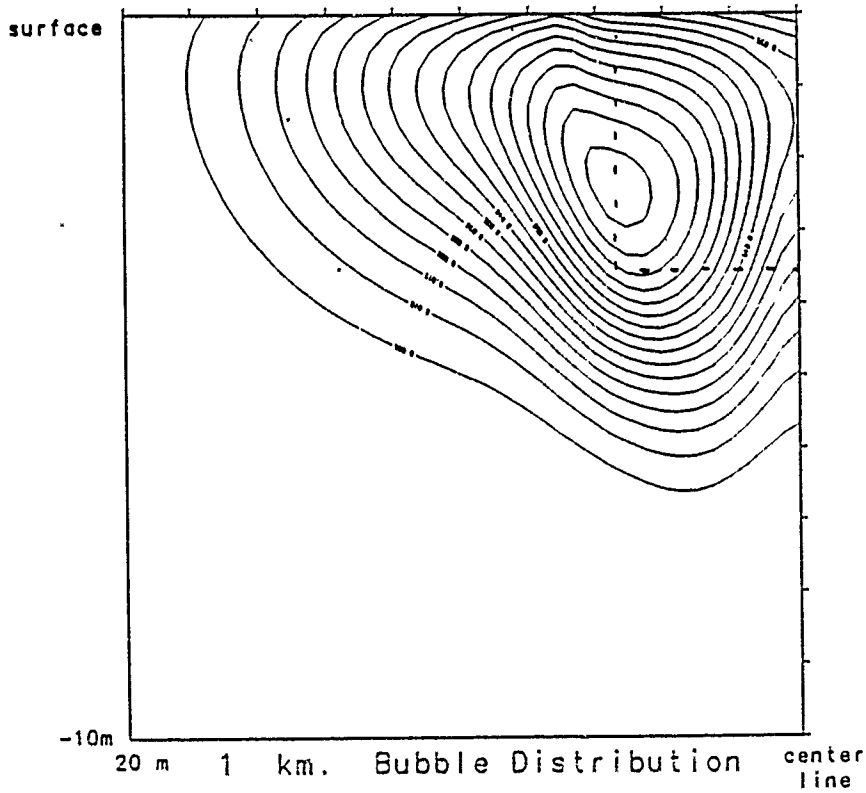

Fig. 5b Full Equations, Pr=.7, 137 microns

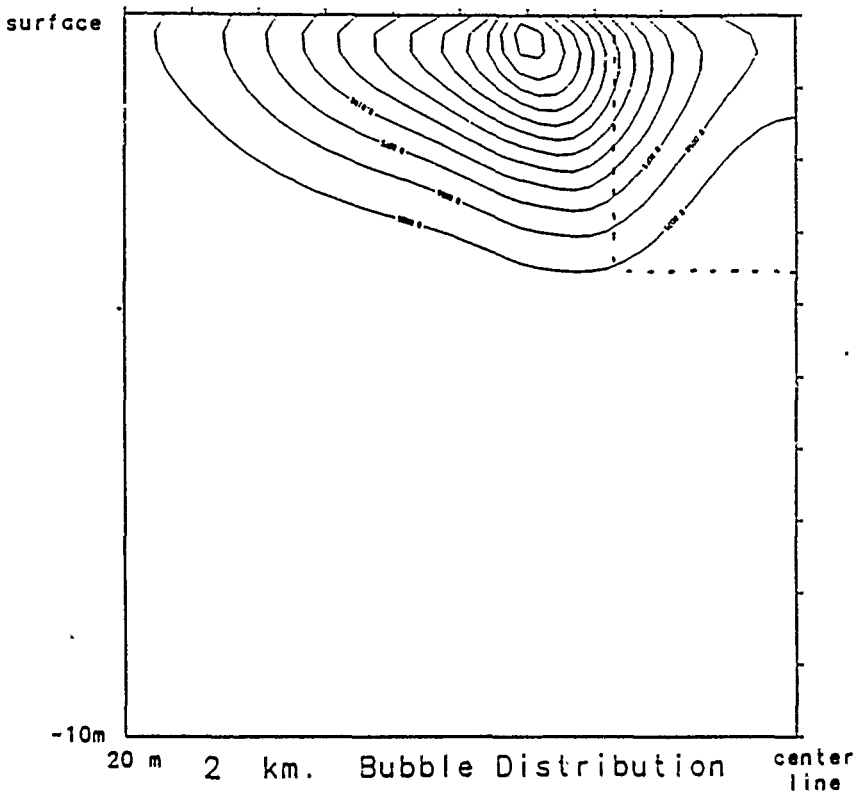

Fig. 5c Full Equations, Pr=.7, 137 microns

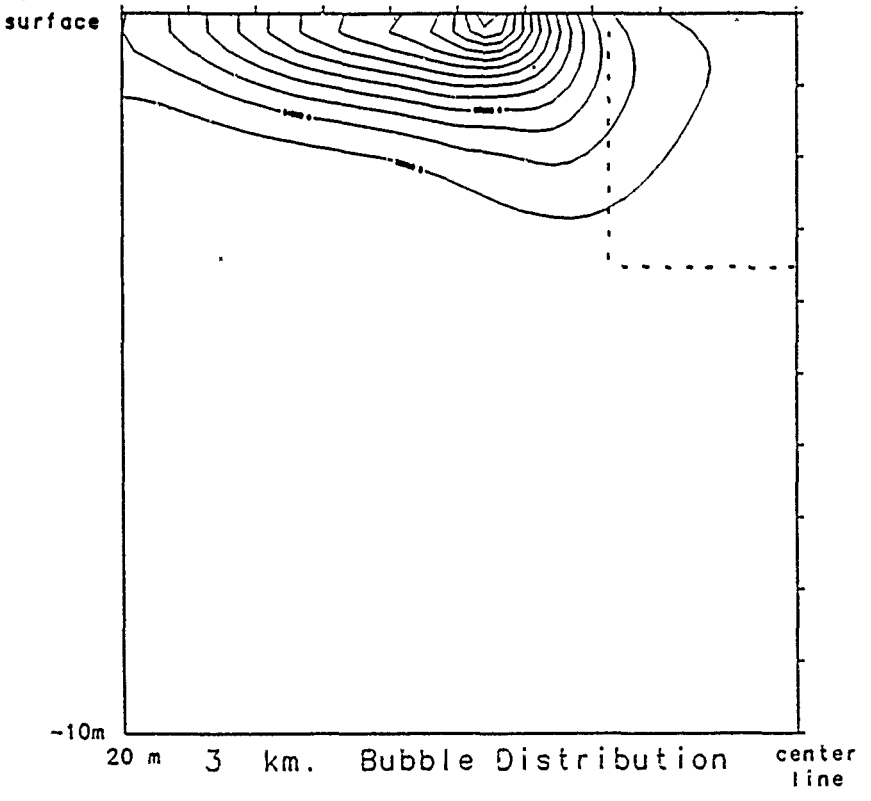

Fig. 5d Full Equations, Pr=.7, 137 microns

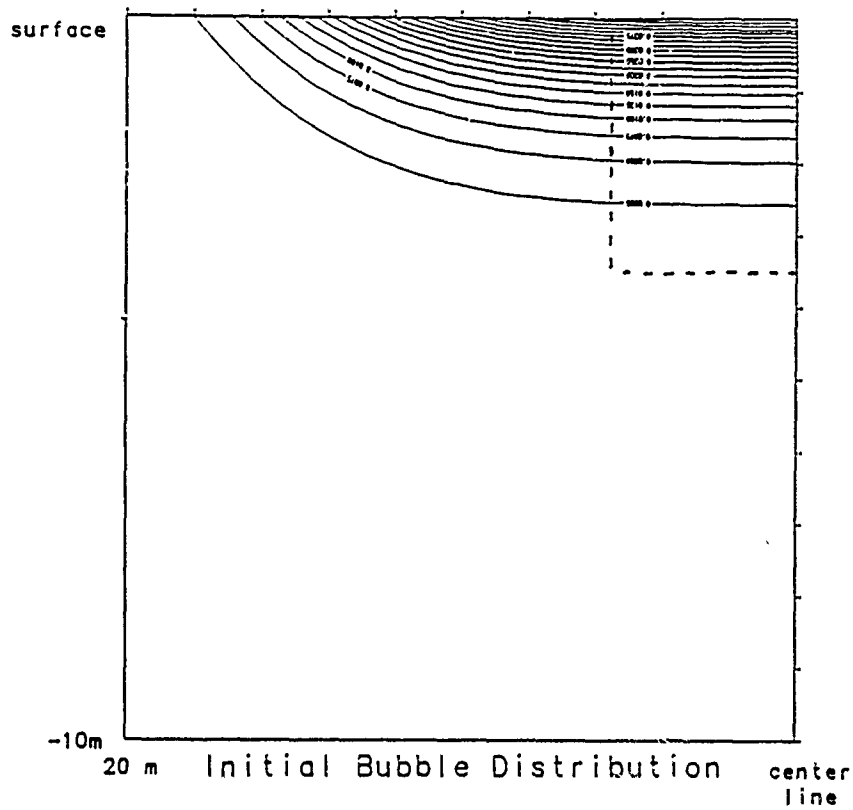

Fig. 6a Full Equations, Pr=.7, 200 microns

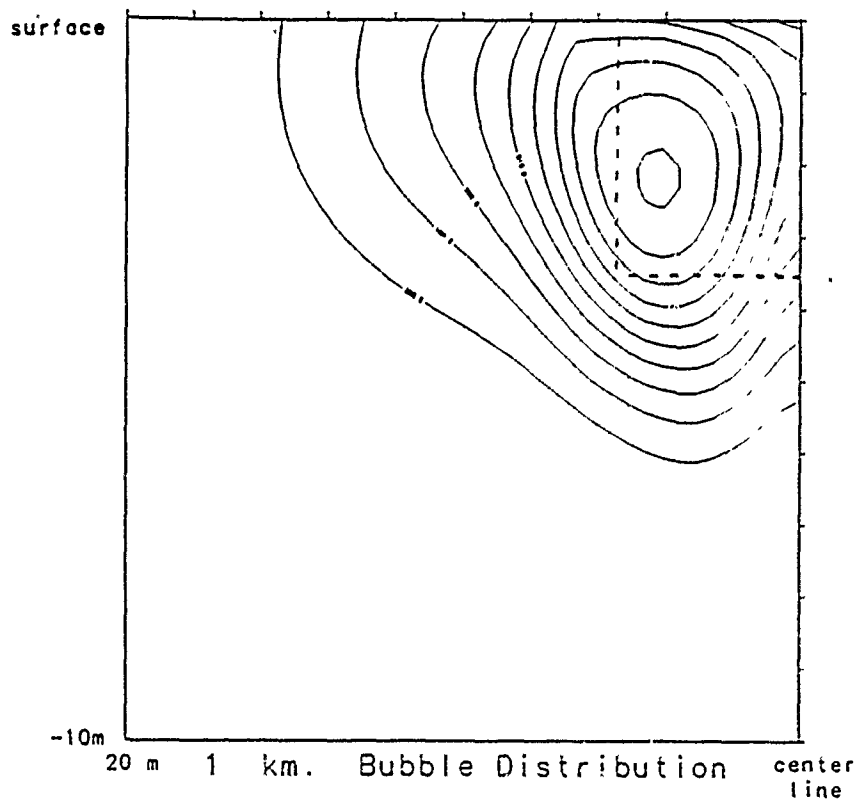

Fig. 6b Full Equations, Pr=.7, 200 microns

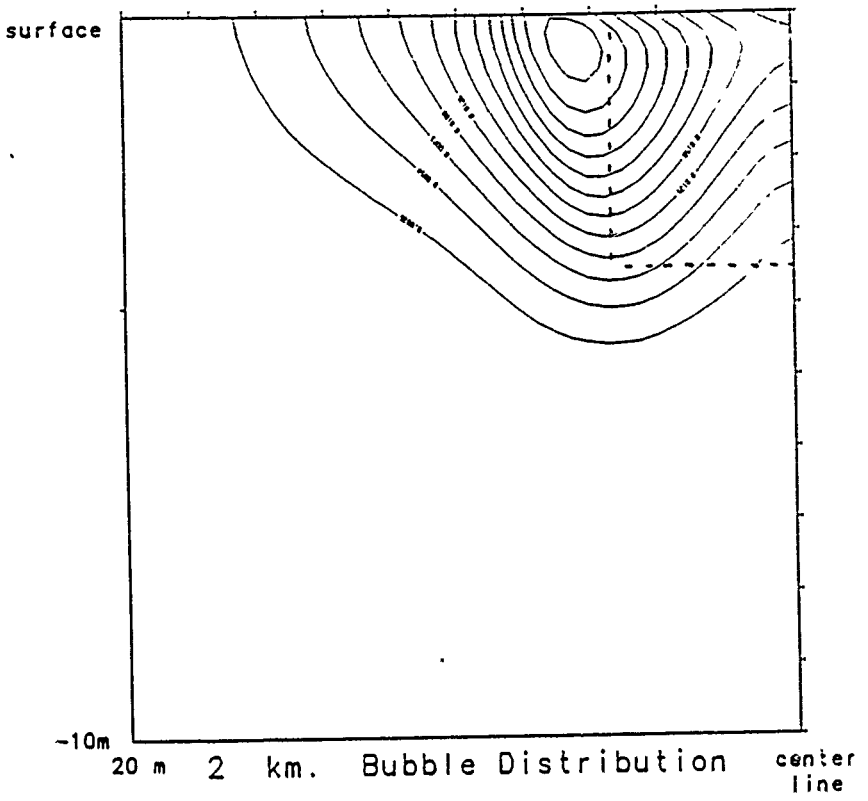

Fig. 6c Full Equations, Pr=.7, 200 microns

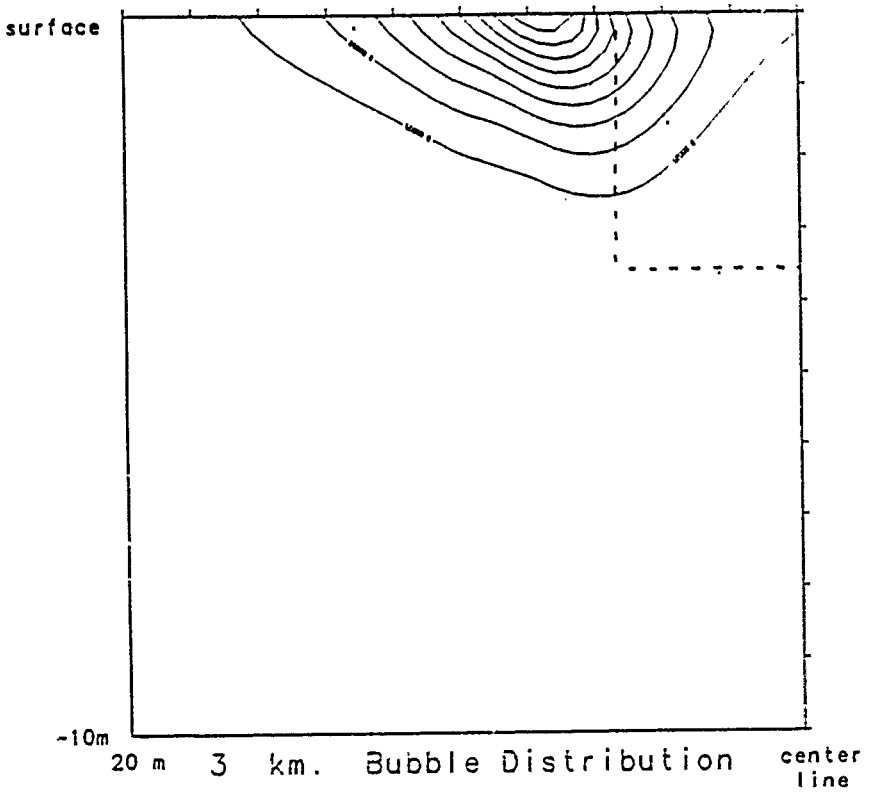

Fig. 6d Full Equations, Pr=.7, 200 microns

and forming a somewhat impermeable barrier or higher gas levels in the water than expected reducing the concentration difference which drives gas diffusion.

The larger bubbles disappear less rapidly because the rate of change of bubble radius via gas diffusion is proportional to the area/volume ratio or 1/r. The larger bubbles are removed by a different mechanism. They rise through the propeller vortex to leave the calculation space at the water surface. For the largest bubble size, 200 microns, they essentially all leave by the 3 km. station. The contributions of each of the terms in the bubble transport equation are not easy to separate in these plots.

The bubble wake appears to be very persistent for the medium sized bubbles and extend much deeper than the initial bubble distribution by a factor of 2 to 3. The bubble distribution becomes concentrated at these sizes as the smaller bubbles dissolve and the larger bubbles rise.

Sensitivity Analysis

Once the baseline predictions are made using all terms of the bubble transport equation, it is interesting to examine the relative importance of the individual terms as a means of determining the dominant mechanisms of bubble motion. The first trial examined the deviation of the predicted bubble transport from a purely convective process. In this case convection is a linear combination of water velocities and steady state rise velocity. Figures 7-11 show bubble distributions at 2 km. caused by pure convective transport. These results can be compared to the relevant results shown in figures 2-6 from the full equations. The smaller bubbles are convected primarily by the propeller swirl because of their small rise velocity. The larger bubbles are convected mostly by their own rise rates. In all cases, we can see the importance of the the non-convective terms in the extent, the structure, and the composition of the bubble wake.

The second trial examined the importance of the empirical turbulent diffusion term. Since there is no direct supporting experimental evidence, a sensitivity analysis is in order. The effective turbulent Prandtl number was decreased by a factor of 3. This value of the Pr number was chosen from the argument that bubbles may respond 3 times more vigorously than neutrally buoyant particles. Figures 12-16 show these results. As expected an increase in turbulent diffusion causes the bubble wake to become significantly larger and less dense. At this time it is not possible to define the correct Prandtl number. It may, in fact be much smaller or larger.

A third trial examined the effect of gas diffusion on the bubble distribution. Figures 17-21 show the effect of eliminating gas diffusion which in some situations may be more realistic than including it. Surfactant films or caps are the likely cause. Here we see

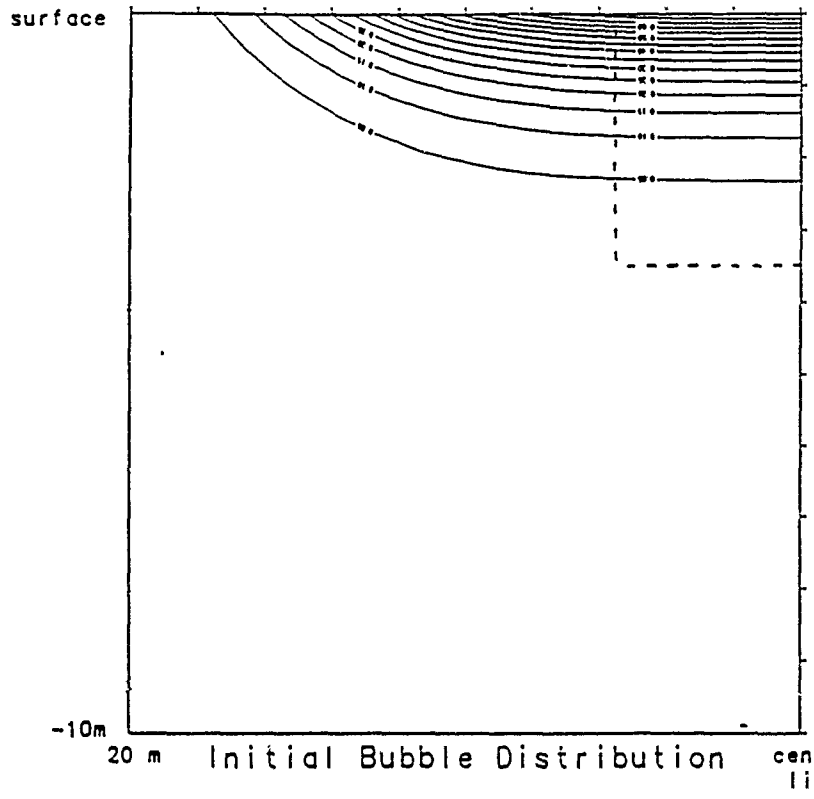

Fig. 7a Convective Motion 10 microns

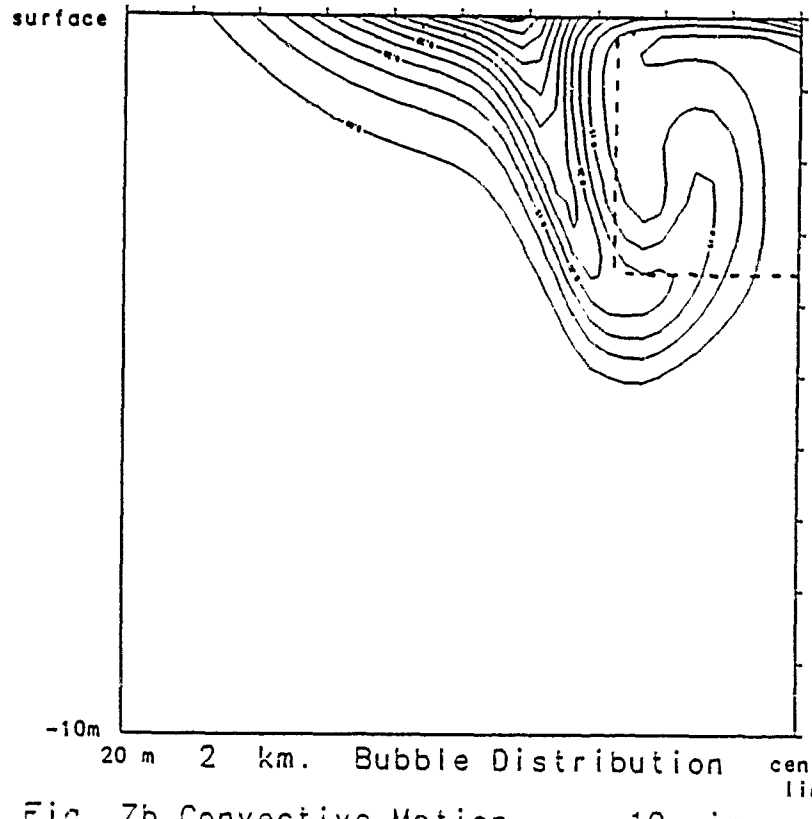

Fig. 7b Convective Motion 10 microns

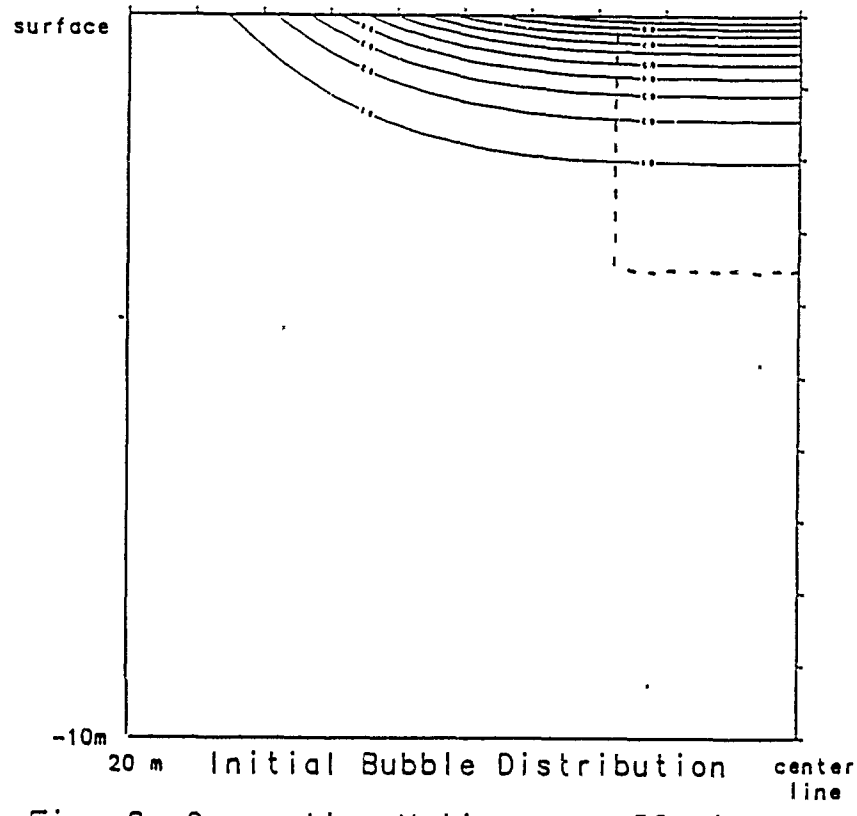

Fig. 8a Convective Motion 52 microns

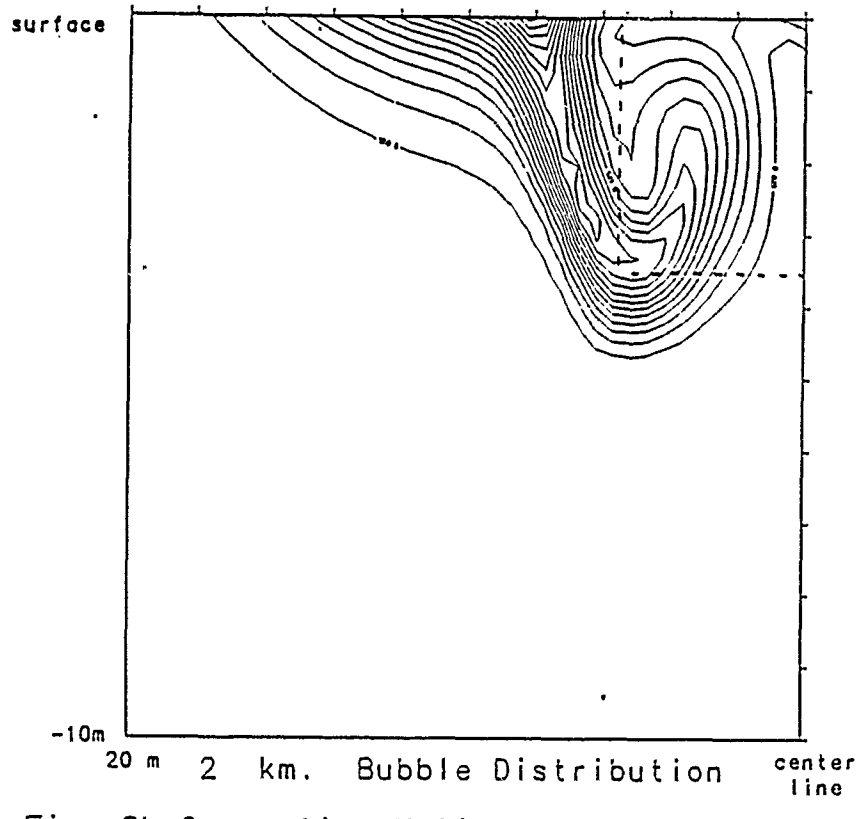

Fig. 8b Convective Motion 52 microns

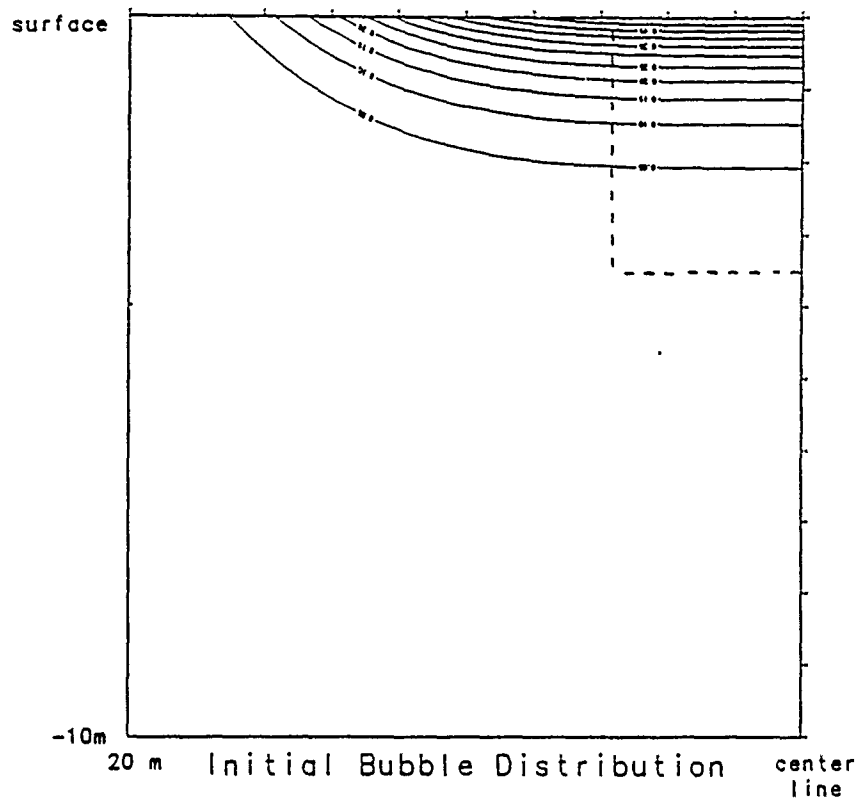

Fig. 9a Convective Motion 94 microns

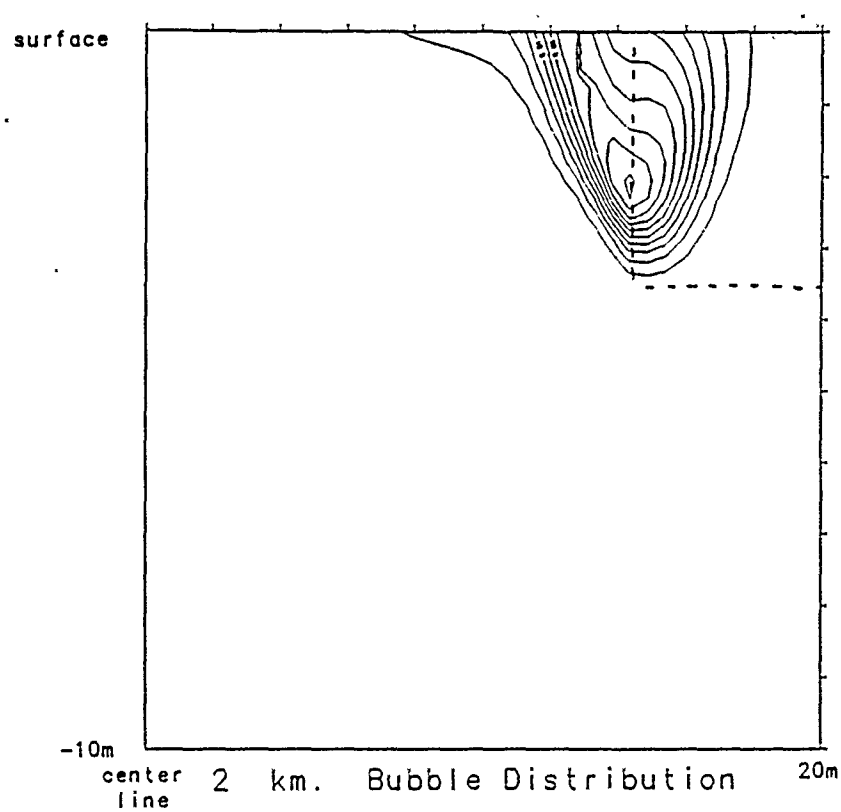

Fig. 9b Convective Motion 94 microns

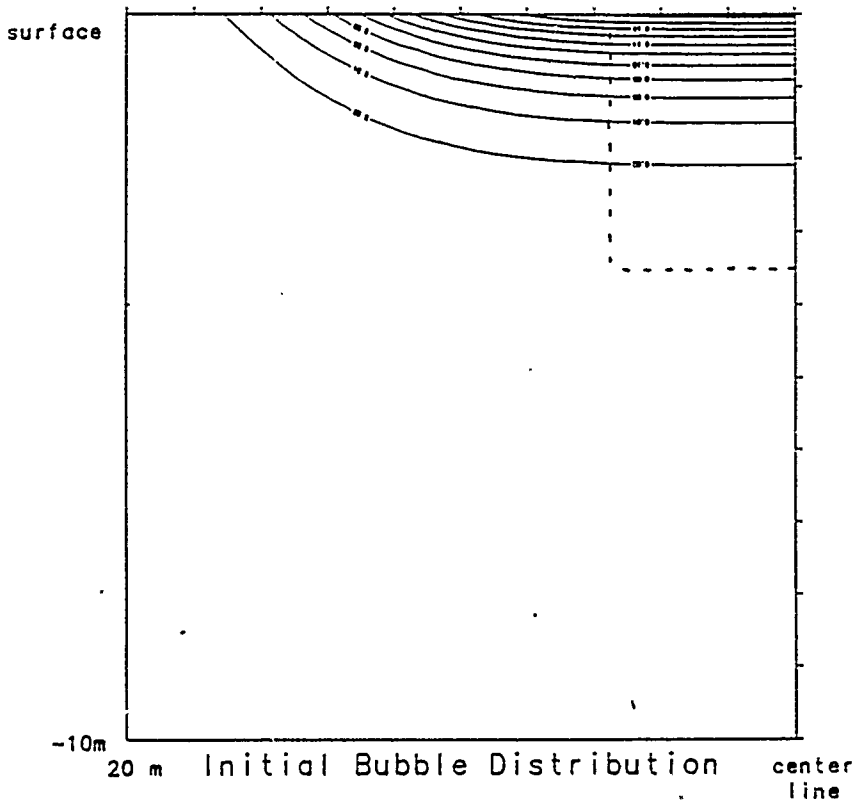

Fig.10a Convective Motion 137 microns

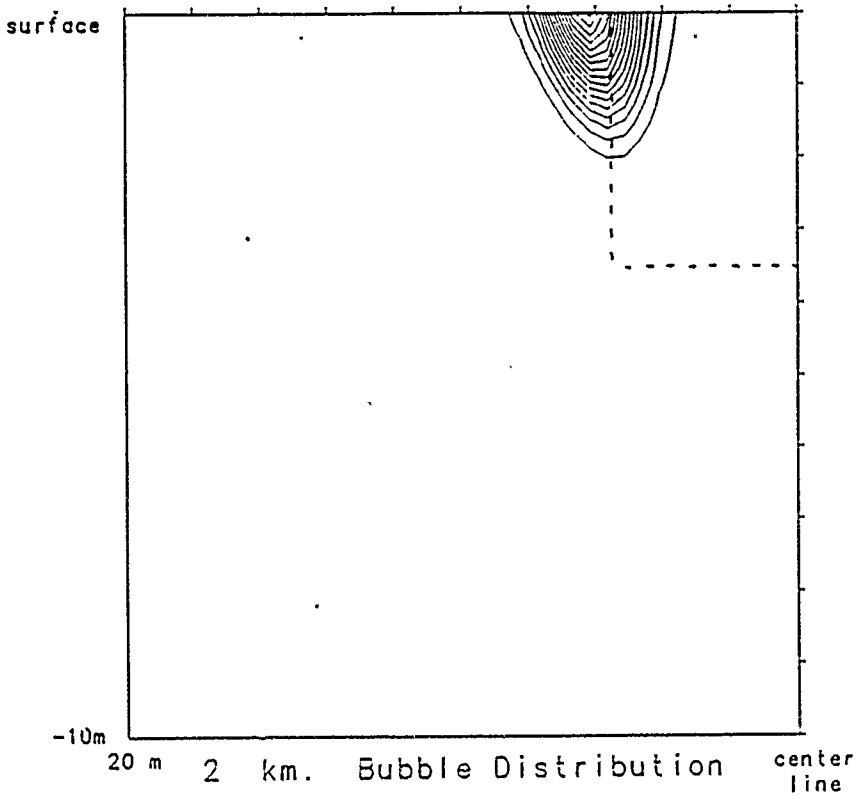

Fig.10b Convective Motion 137 microns

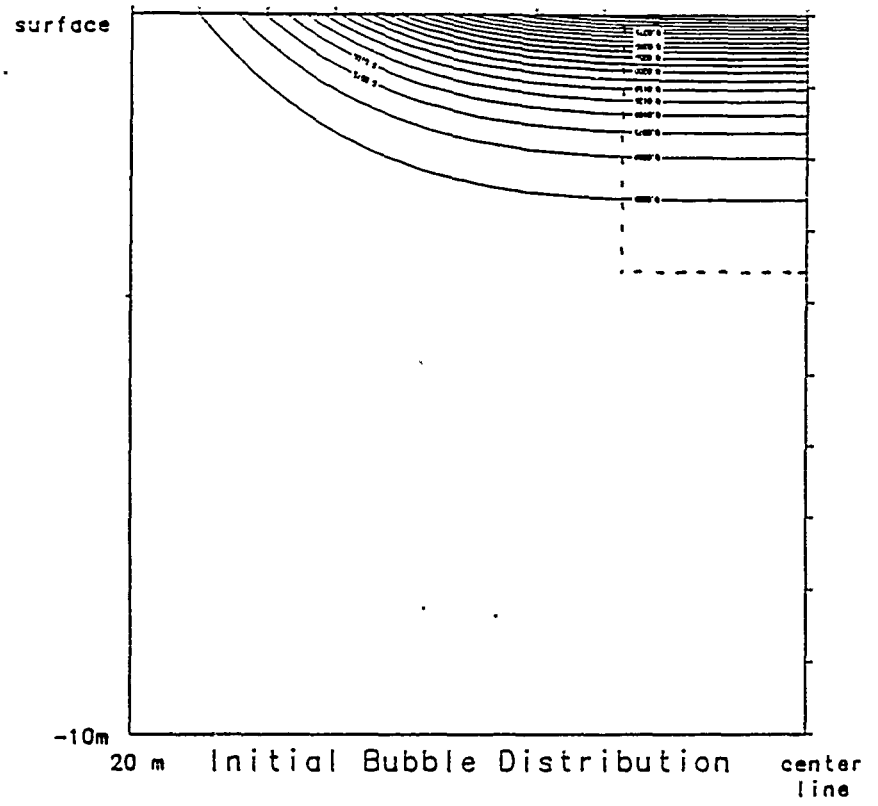

Fig.11a Convective Motion 200 microns

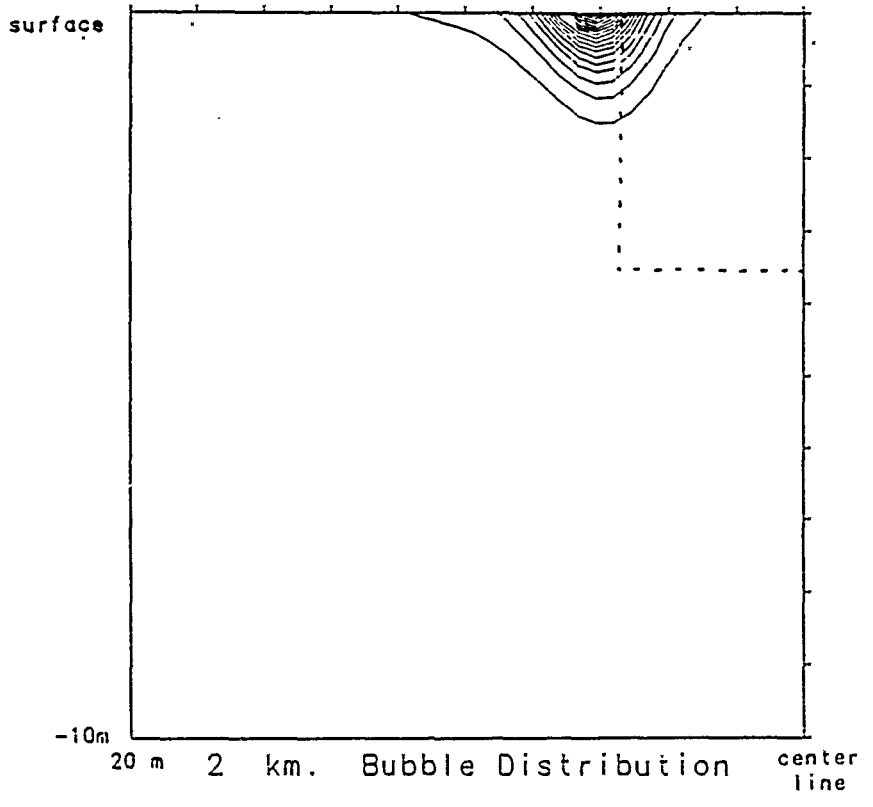

Fig.11b Convective Motion 200 microns

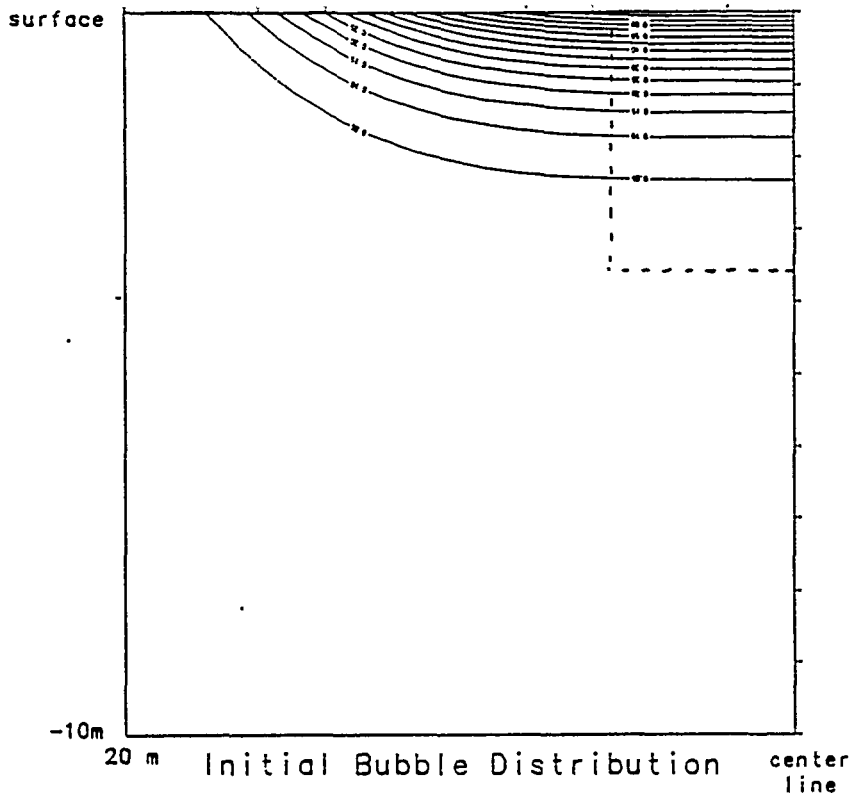

Fig.12a Full Equations, Pr=.23, 10 microns

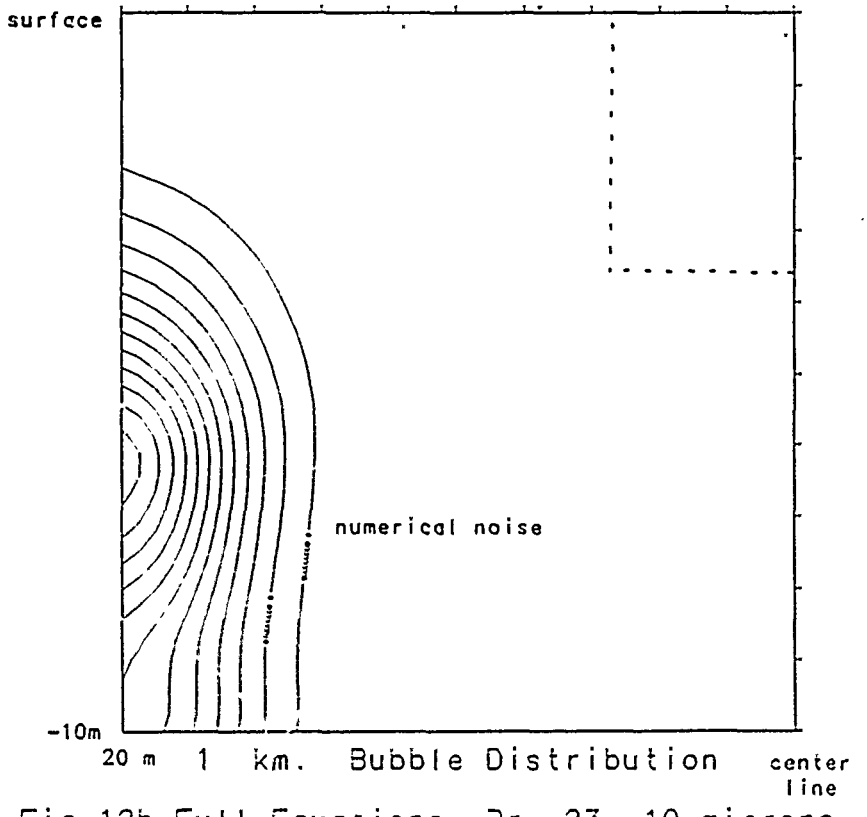

Fig.12b Full Equations, Pr=.23, 10 microns

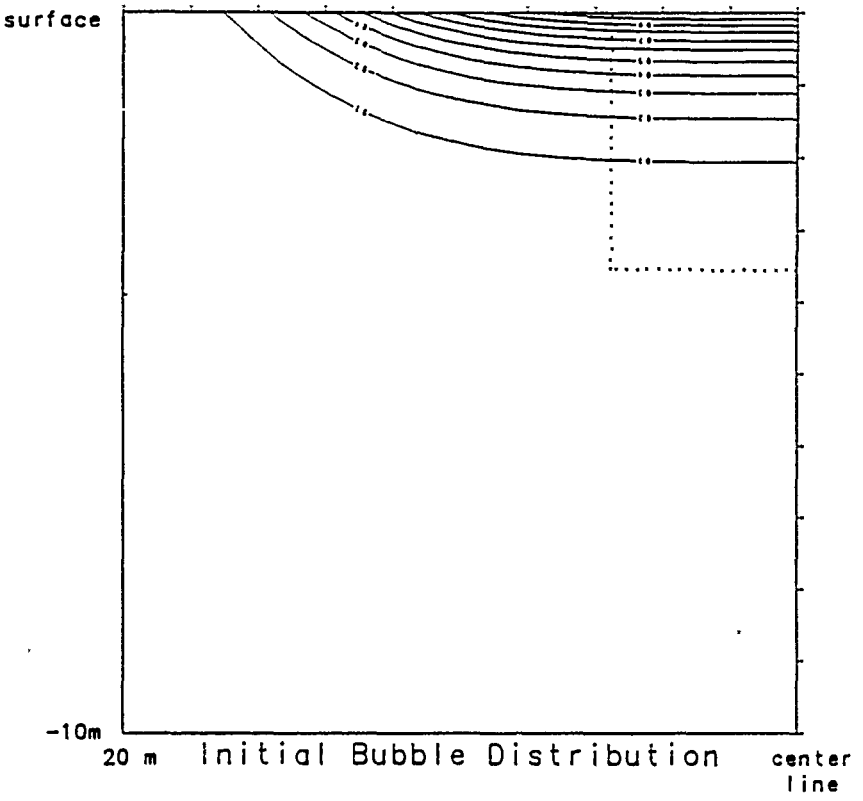

Fig.13a Full Equations, Pr=.23, 52 microns

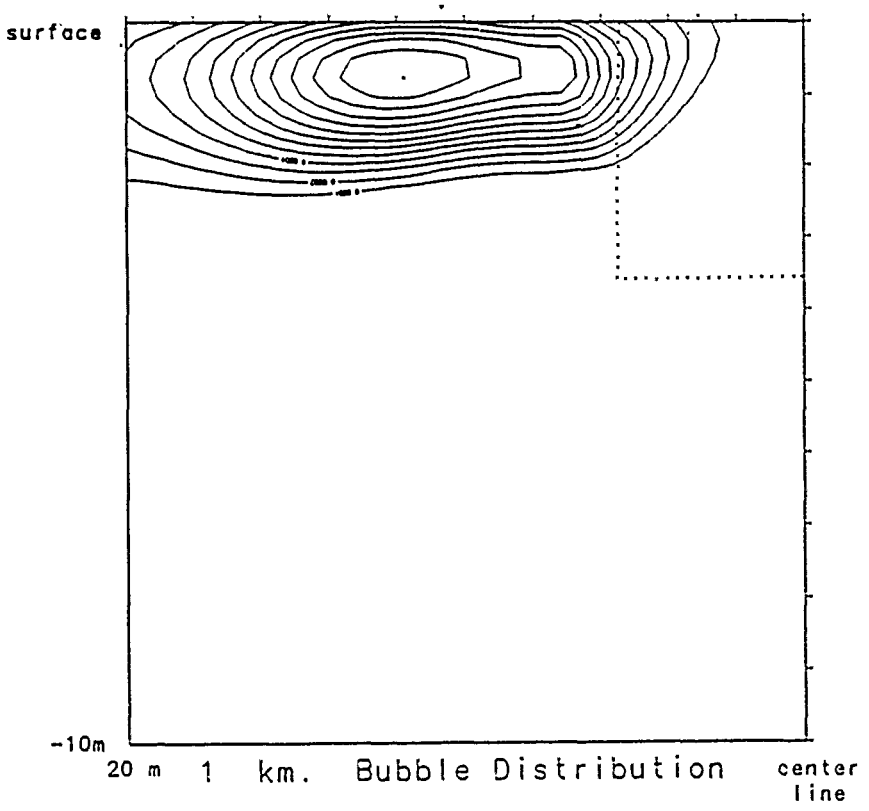

Fig.13b Full Equations, Pr=.23, 52 microns

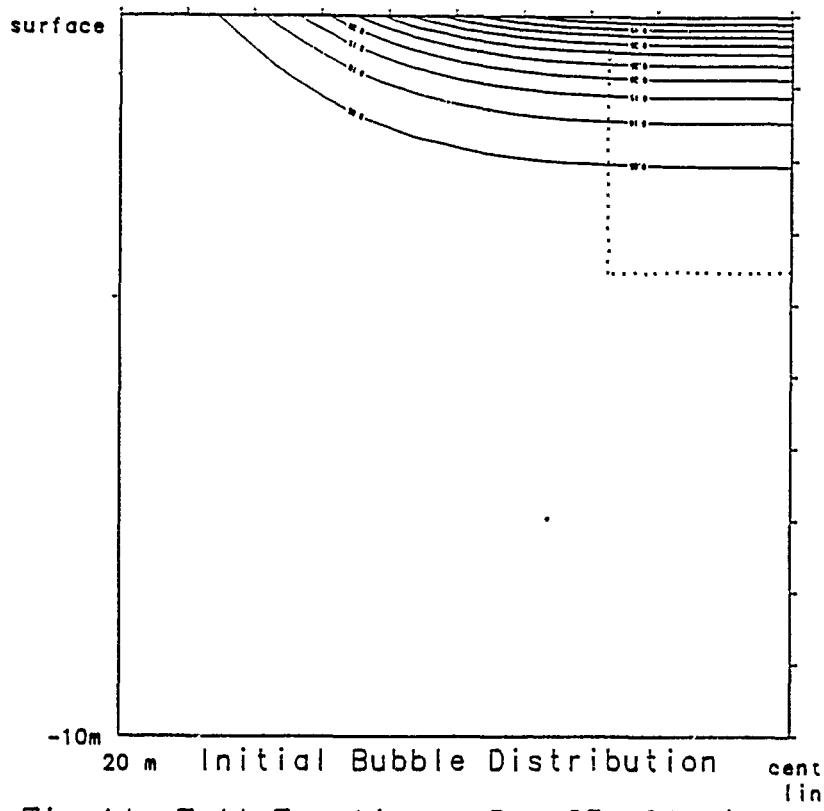

Fig.14a Full Equations, Pr=.23, 94 microns

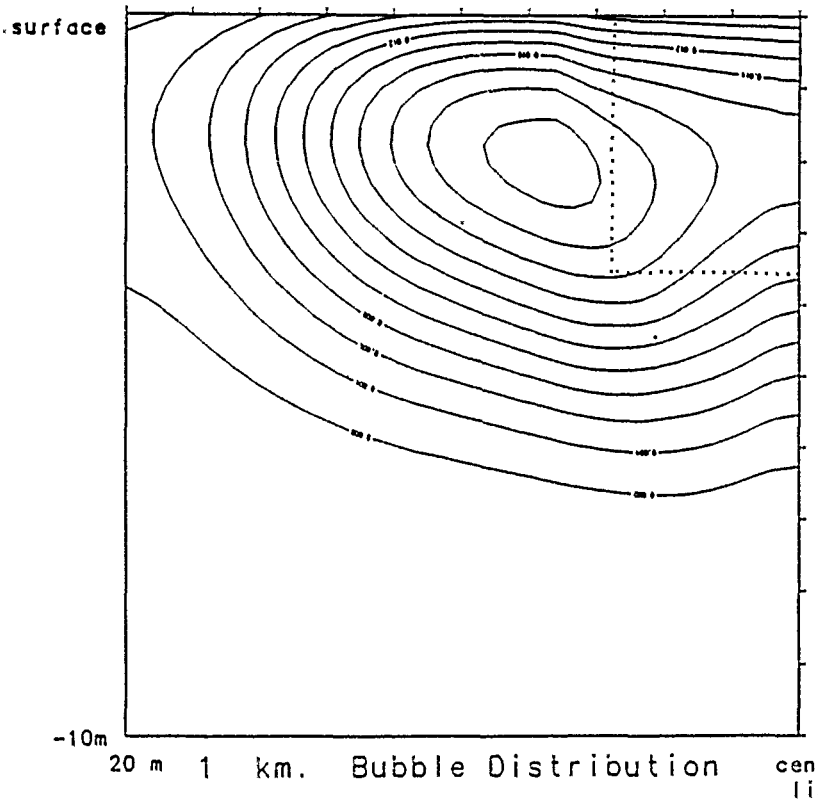

Fig.14b Full Equations, Pr=.23, 94 microns

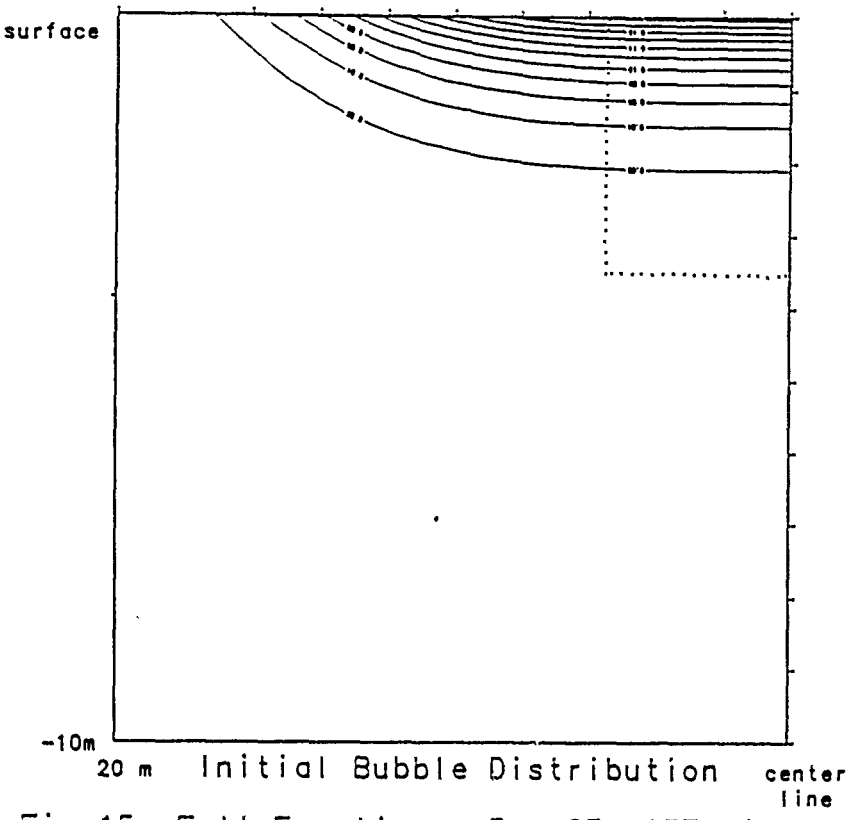

Fig.15a Full Equations, Pr=.23, 137 microns

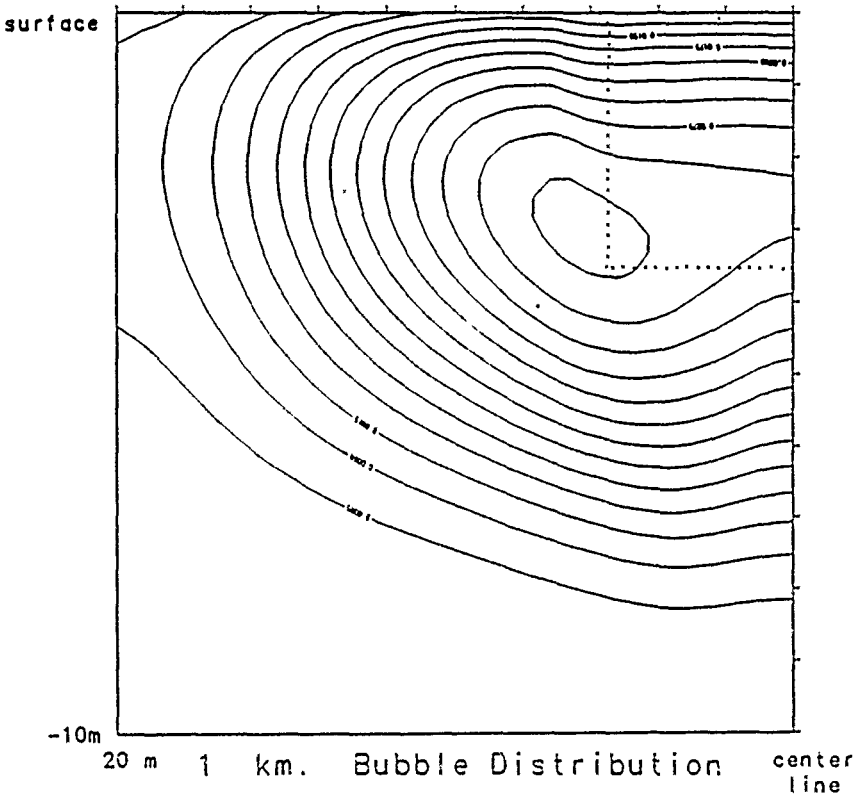

Fig.15b Full Equations, Pr=.23, 137 microns

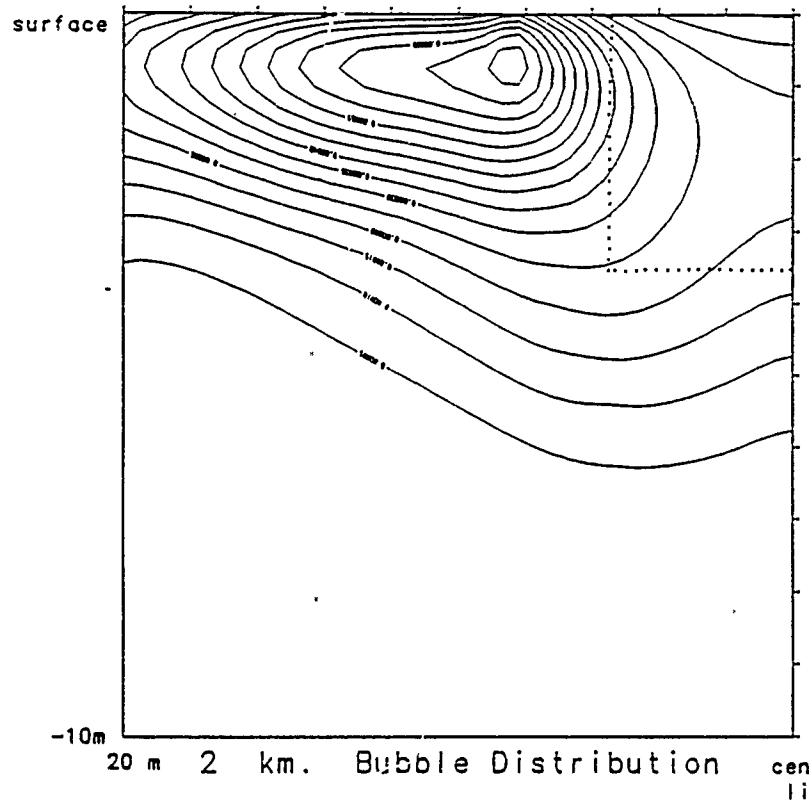

Fig.15c Full Equations, Pr=.23, 137 microns

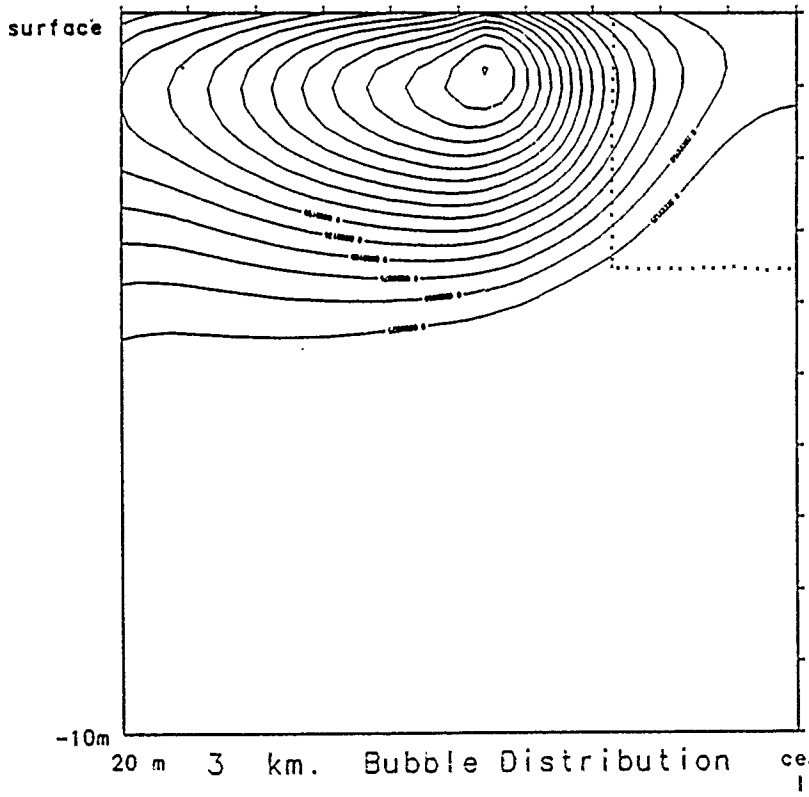

Fig.15d Full Equations, Pr=.23, 137 microns

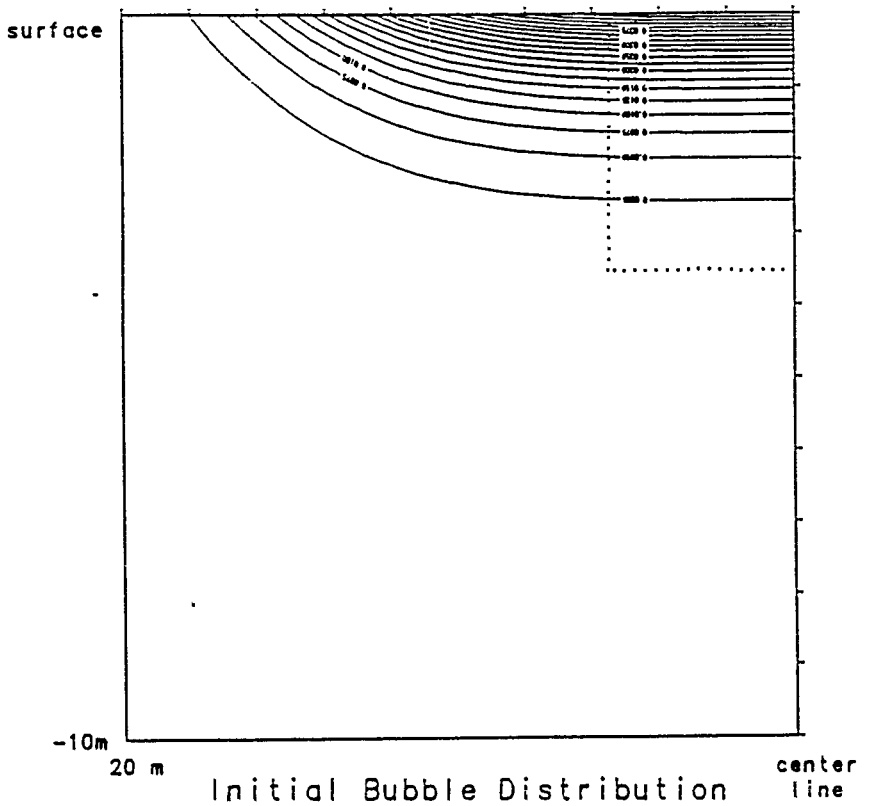

Fig.16a Full Equations, Pr=.23, 200 microns

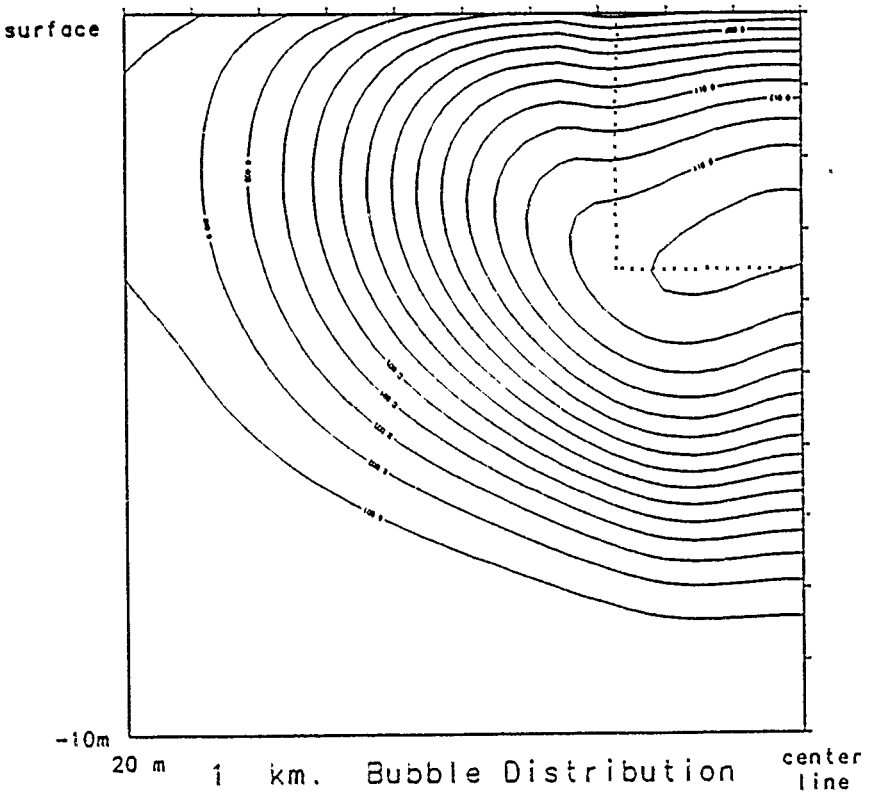

Fig.16b Full Equations, Pr=.23, 200 microns

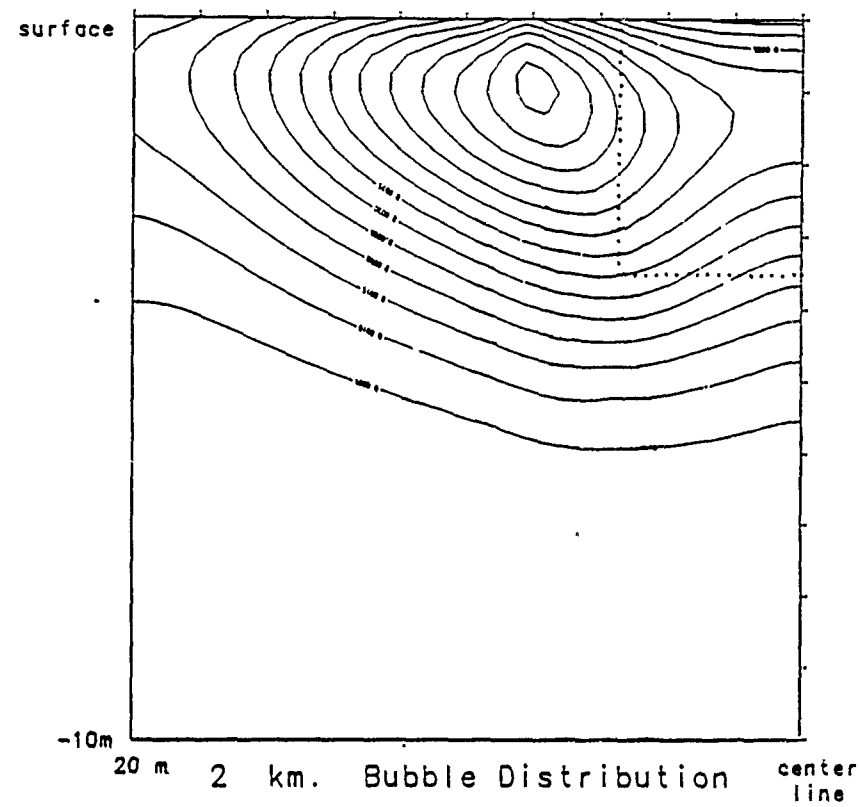

Fig.16c Full Equations, Pr=.23, 200 microns

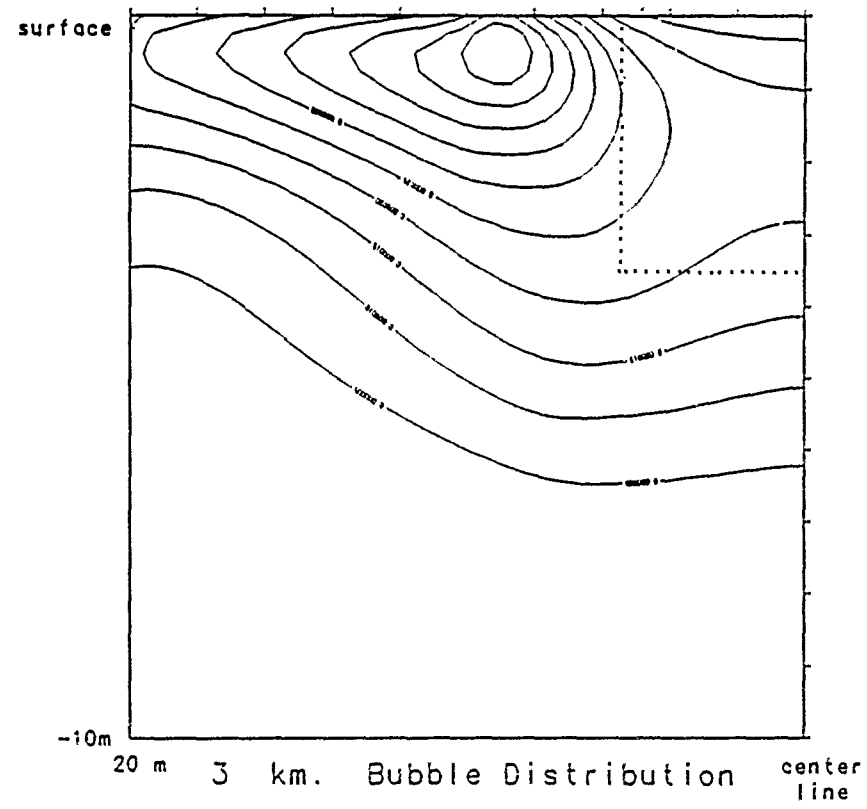

Fig.16d Full Equations, Pr=.23, 200 microns

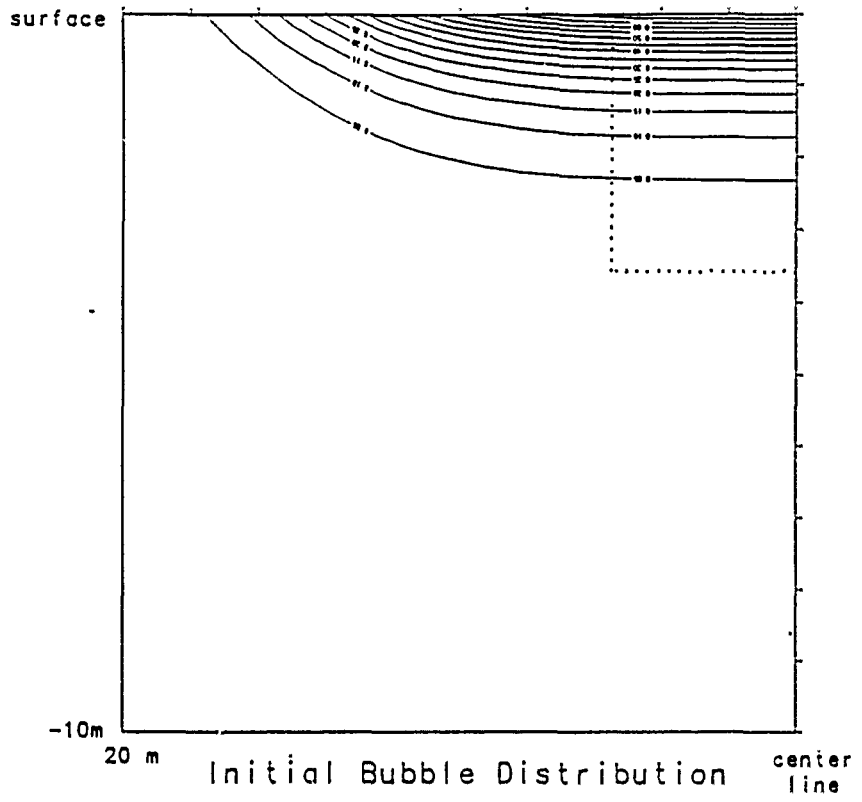

Fig.17a No Gas Diffusion, Pr=.7
10 microns

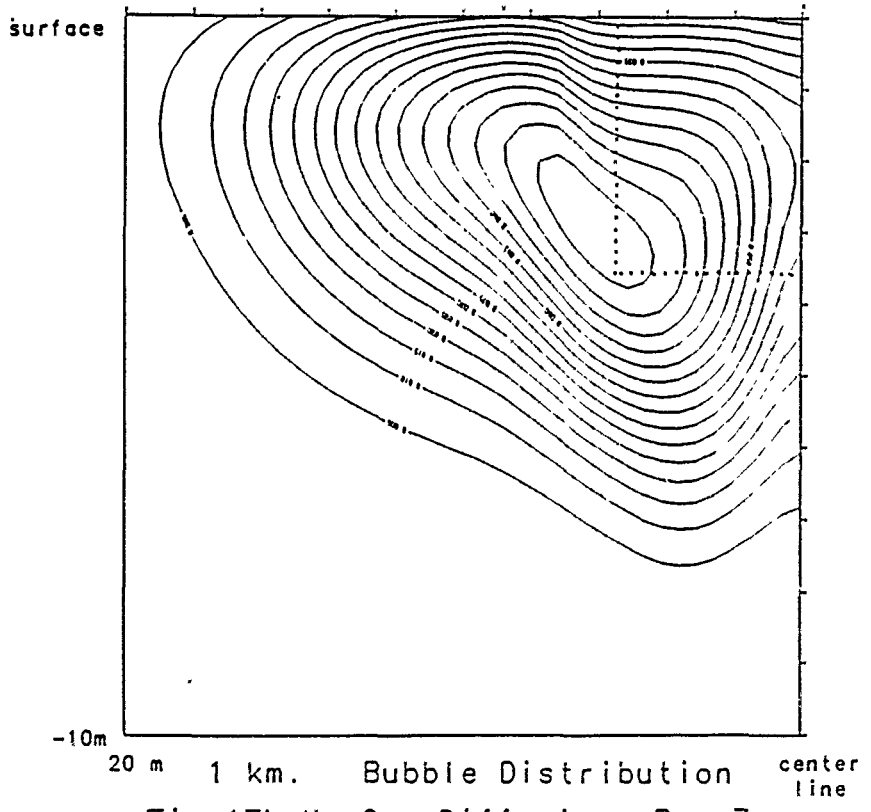

Fig.17b No Gas Diffusion, Pr=.7
10 microns

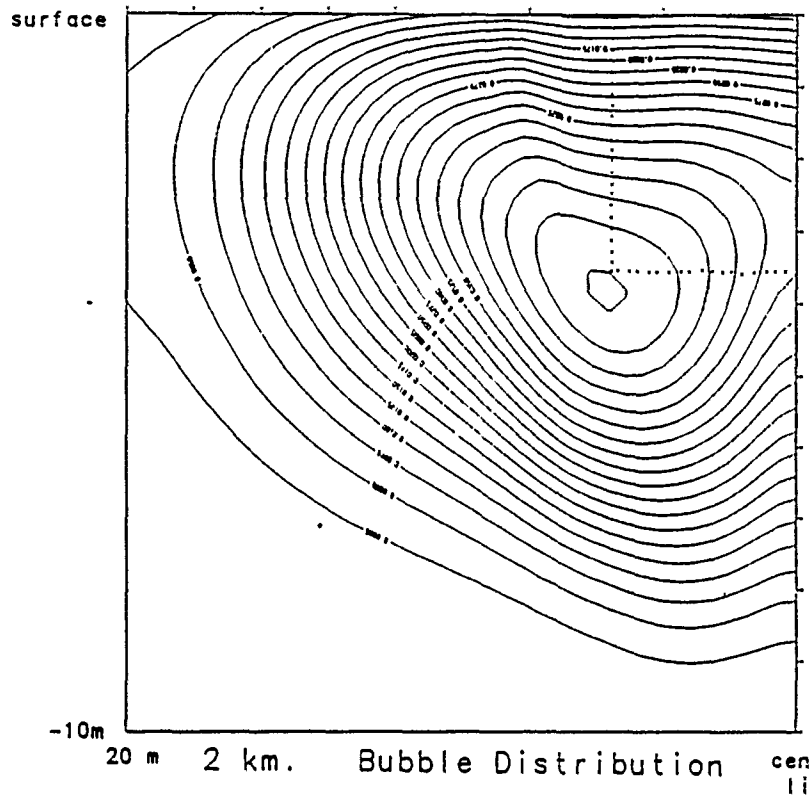

Fig.17c No Gas Diffusion, Pr=.7
10 microns

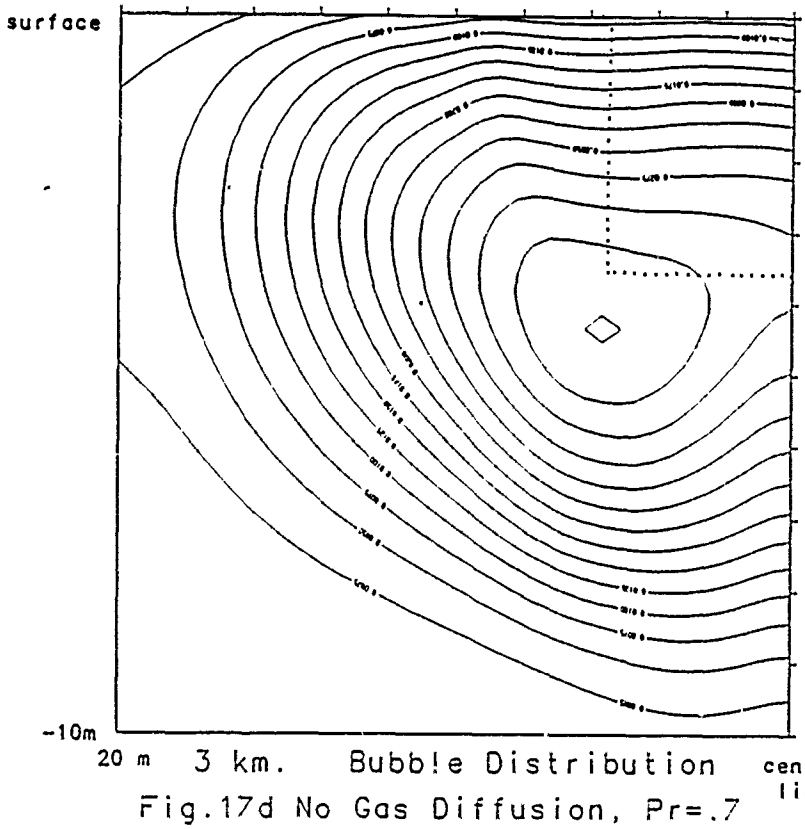

Fig.17d No Gas Diffusion, Pr=.7
10 microns

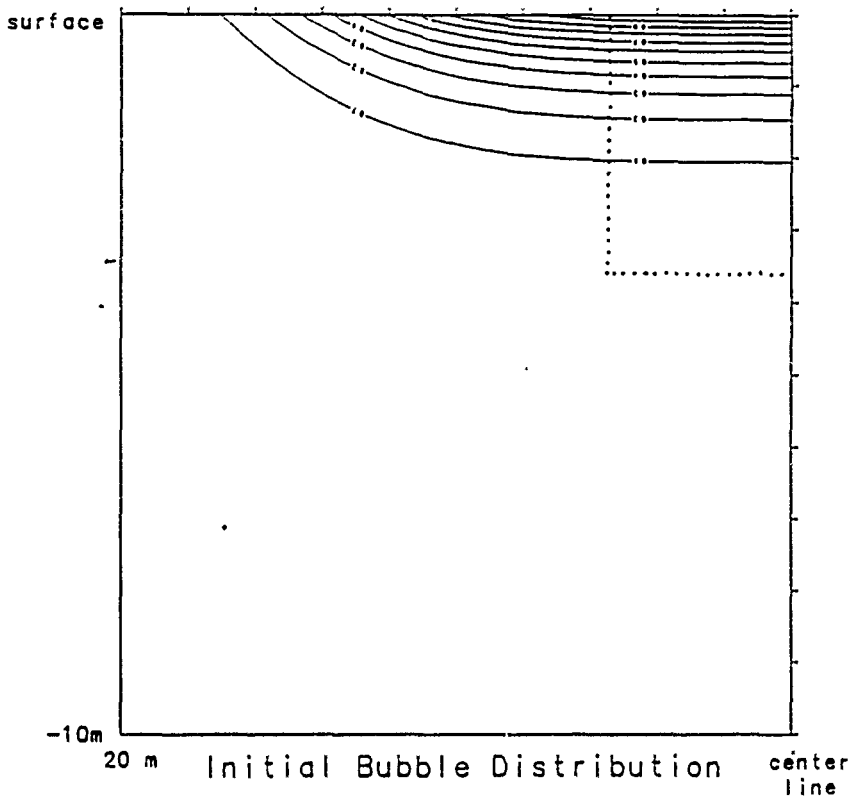

Fig.18a No Gas Diffusion, Pr=.7
52 microns

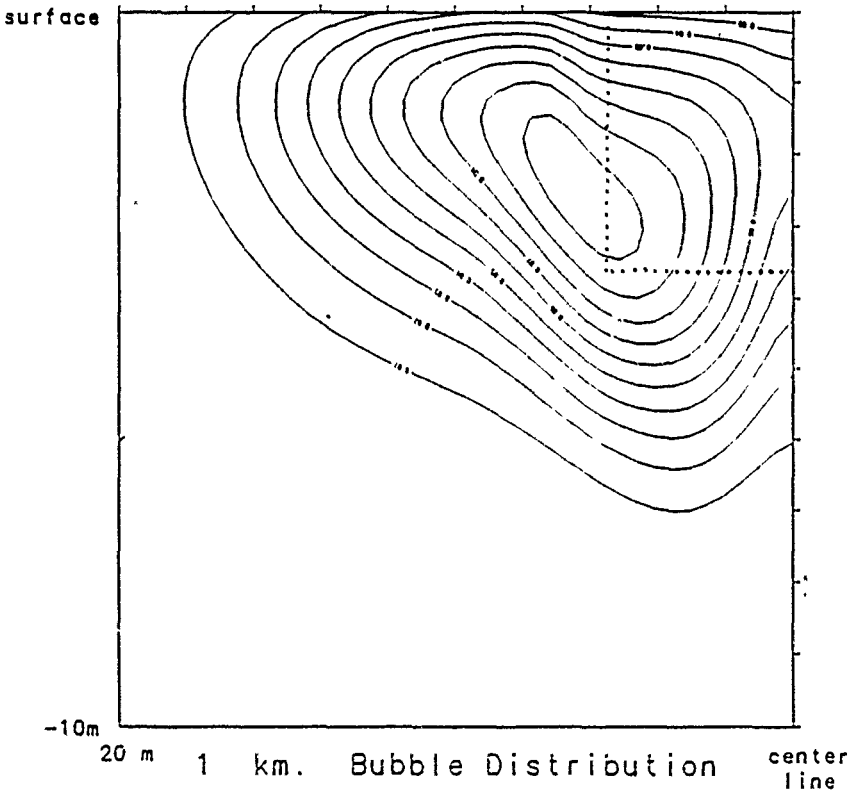

Fig.18b No Gas Diffusion, Pr=.7
52 microns

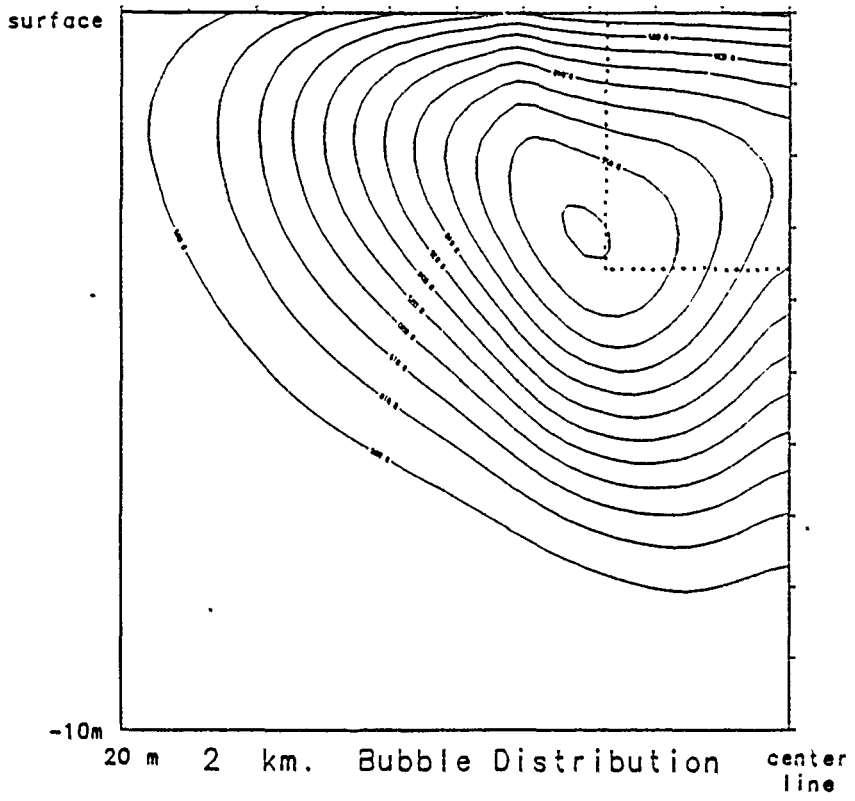

Fig.18c No Gas Diffusion, Pr=.7
52 microns

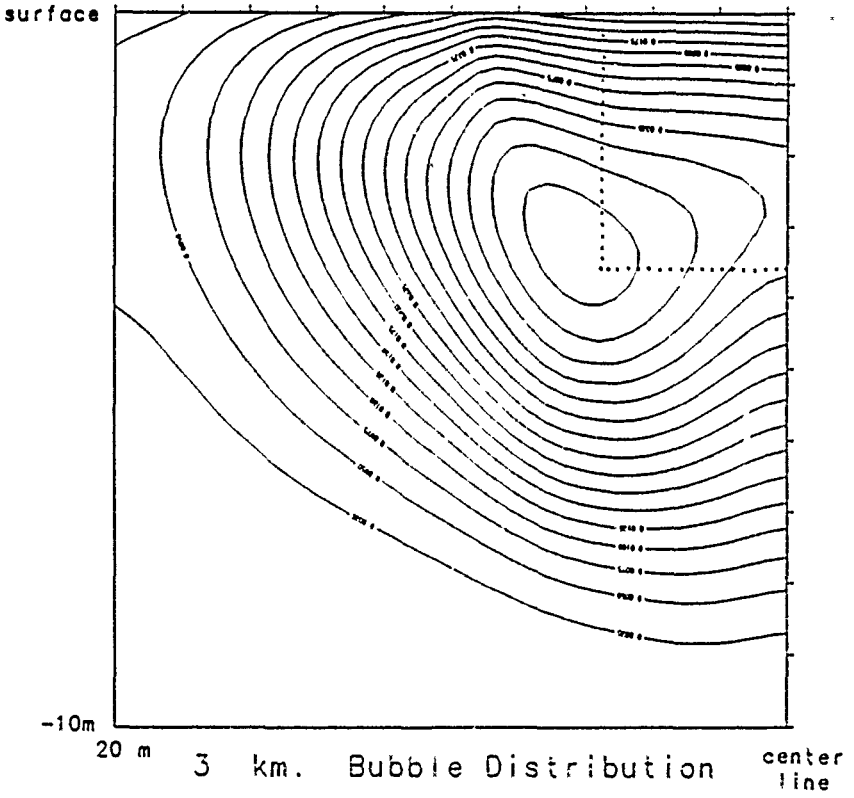

Fig.18d No Gas Diffusion, Pr=.7
52 microns

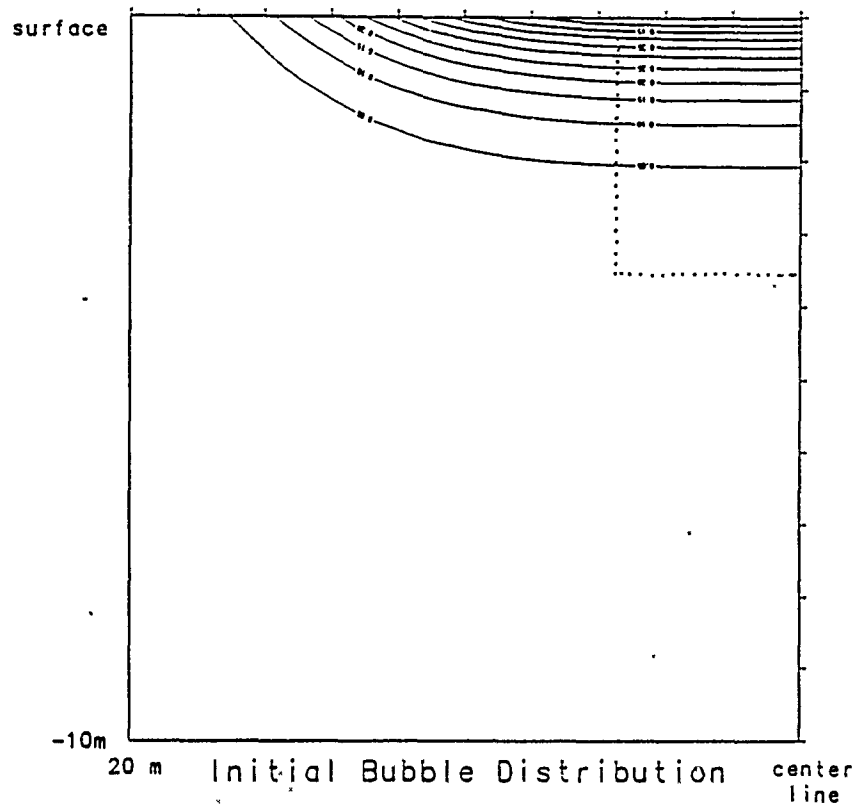

Fig.19a No Gas Diffusion, Pr=.7
94 microns

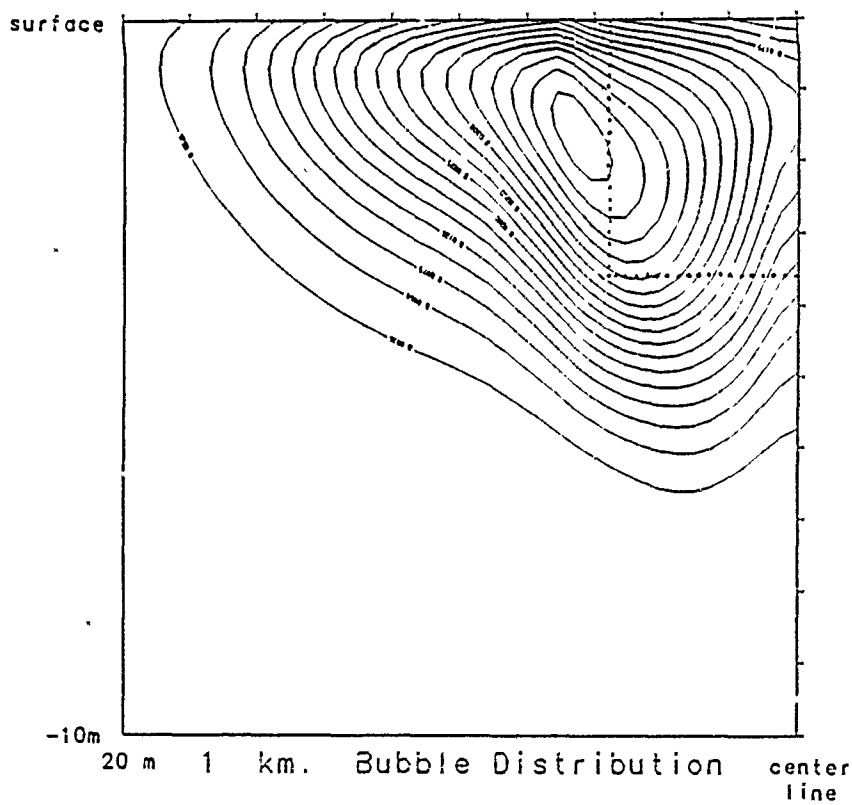

Fig.19b No Gas Diffusion, Pr=.7
94 microns

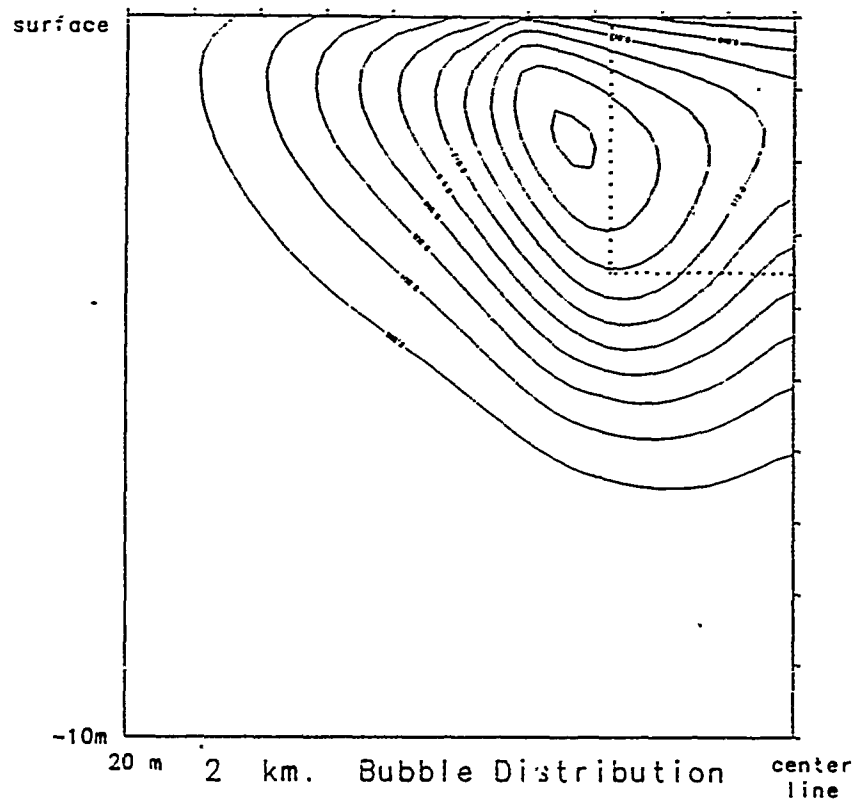

Fig.19c No Gas Diffusion, Pr=.7
94 microns

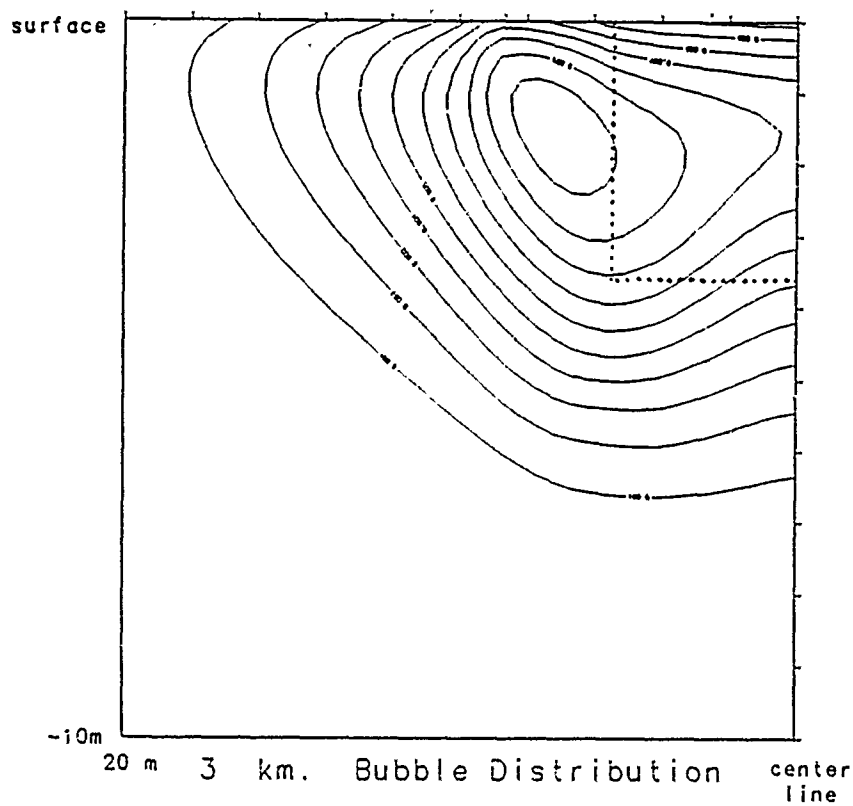

Fig.19d No Gas Diffusion, Pr=.7
94 microns

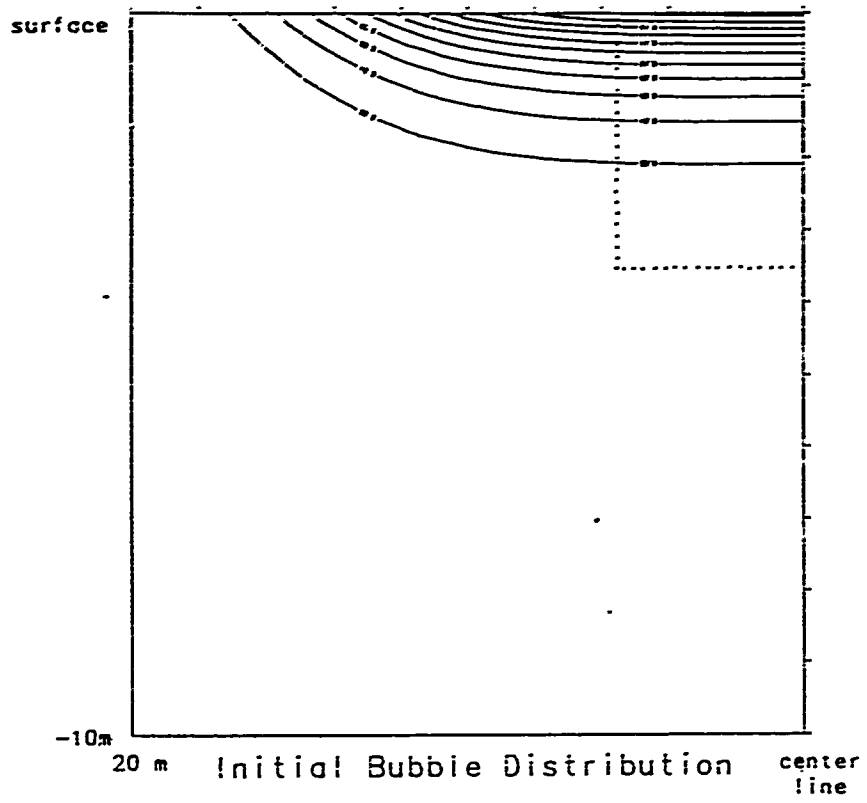

Fig.20a No Gas Diffusion, Pr=.7
137 microns

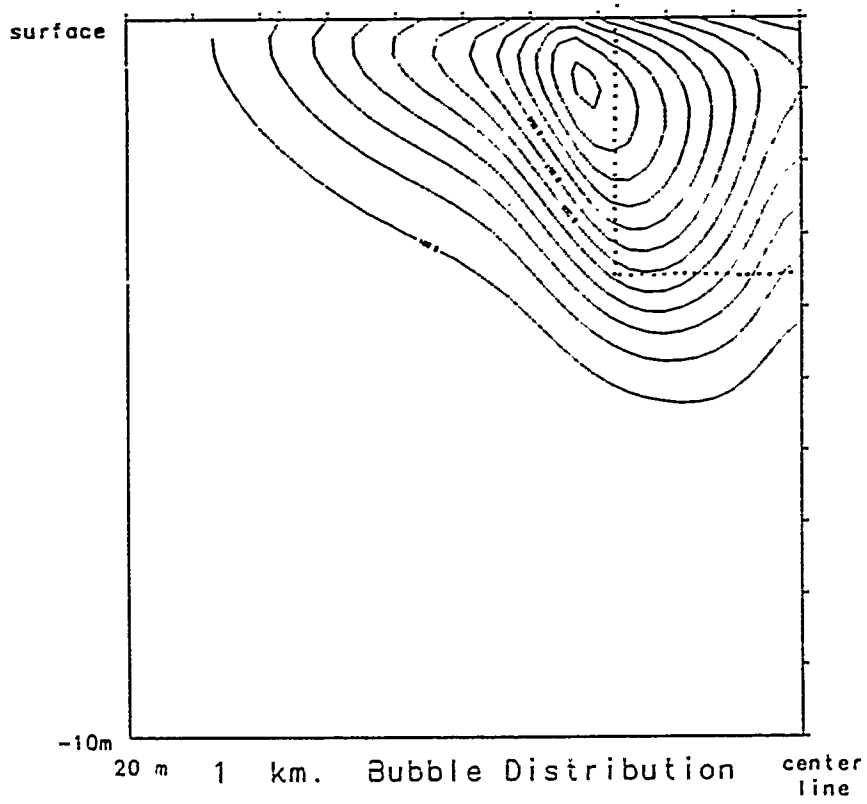

Fig.20b No Gas Diffusion, Pr=.7
137 microns

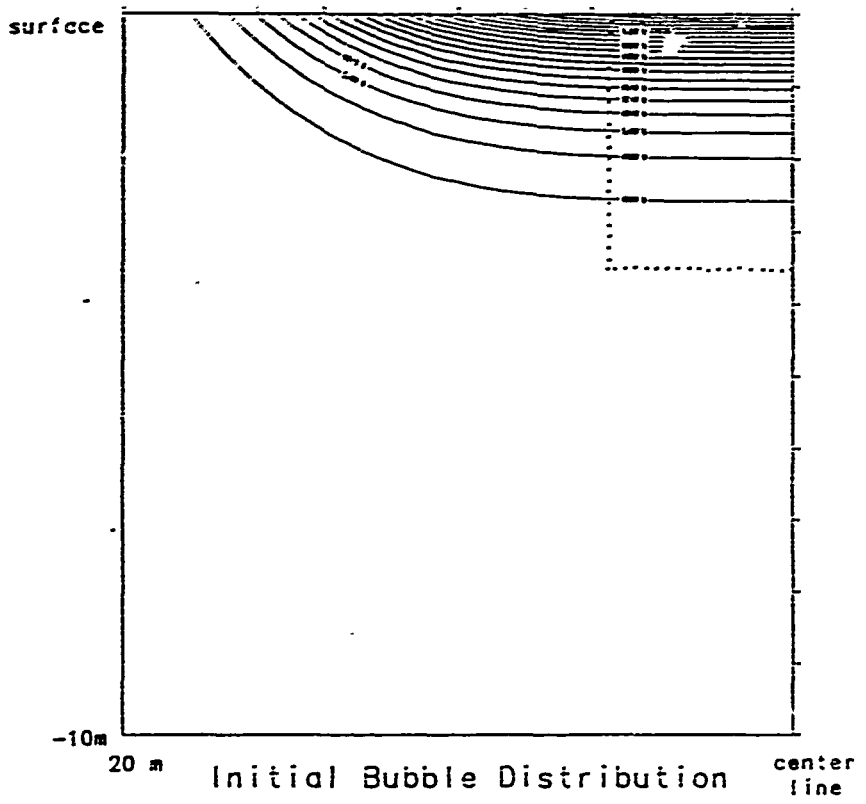

Fig.21a No Gas Diffusion, Pr=.7
200 microns

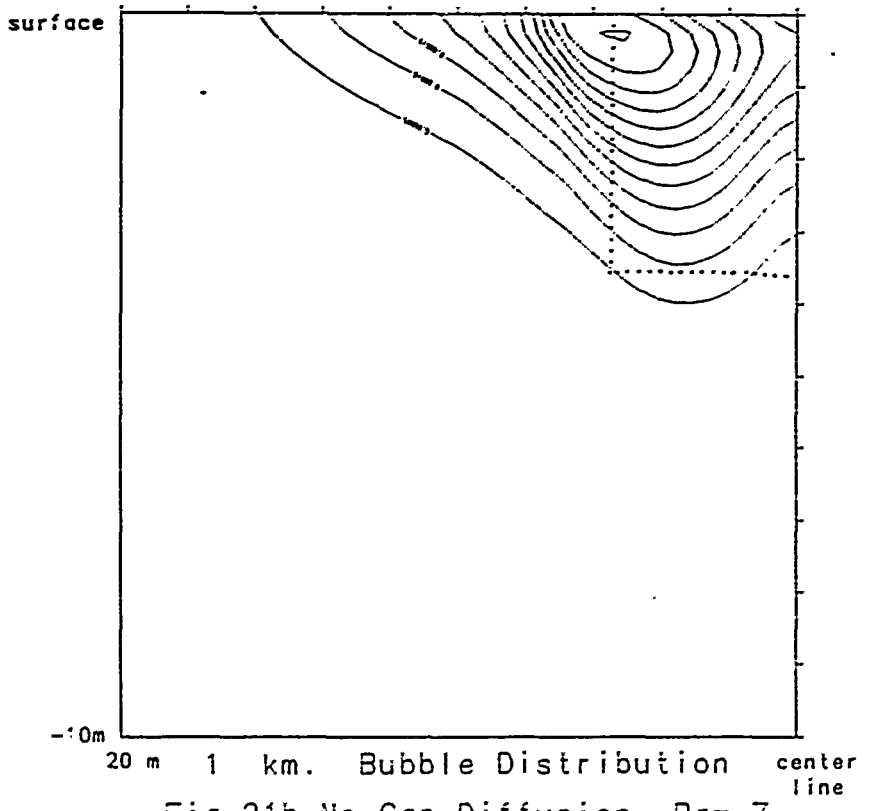

Fig.21b No Gas Diffusion, Pr=.7
200 microns

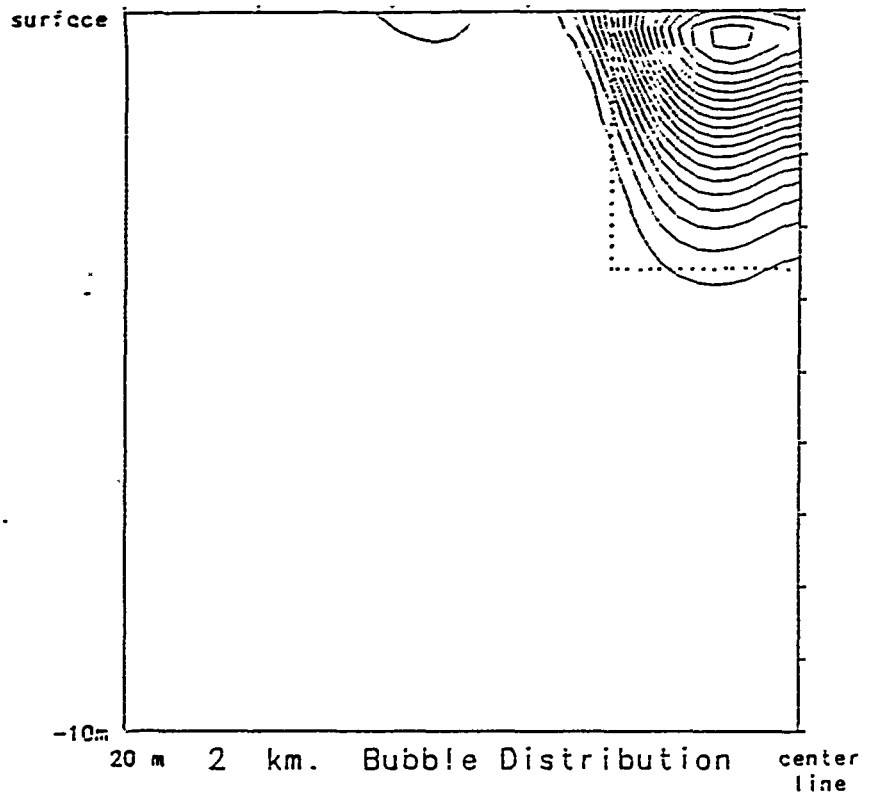

Fig.21c No Gas Diffusion, Pr=.7
200 microns

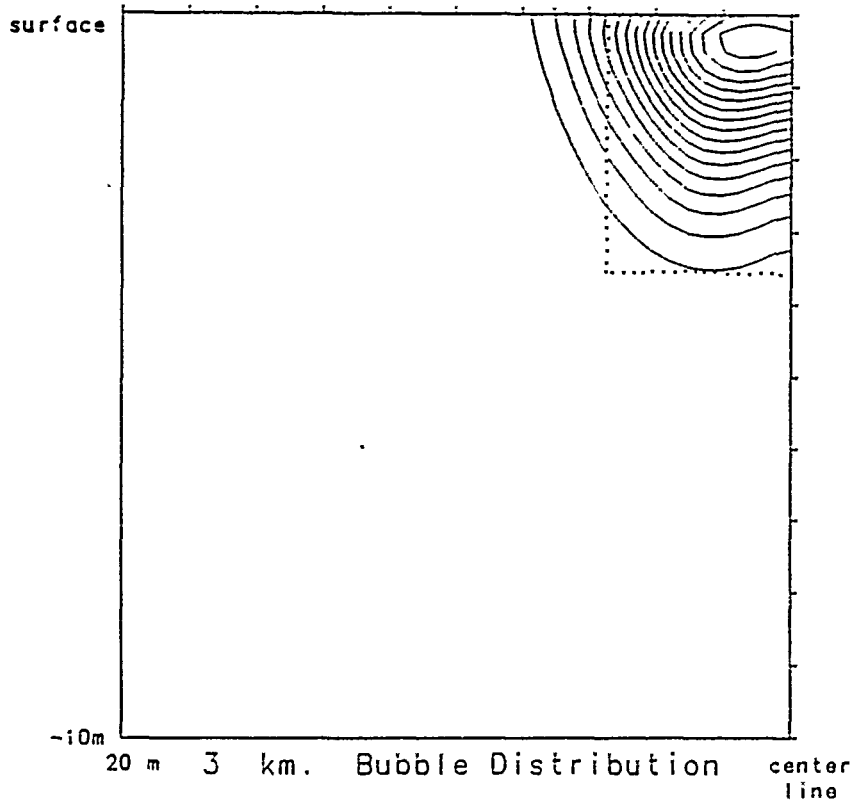

Fig.21d No Gas Diffusion, Pr=.7
200 microns

the smaller bubbles expand to fill the calculation area with essentially no means of removal. There is even a noticeable effect on the largest bubbles.

In summary, it appears that no single effect dominates bubble transport. Gas diffusion, turbulent diffusion, and convective influences are all important. In addition, there is considerable uncertainty concerning the coefficients used in modeling these effects in real situations. A comprehensive model of the bubble wake will require better experimental foundations on the magnitude of the individual effects.

In addition, there are possible additional effects not considered here. Bubbles can behave very differently than high density particles in the presence of pressure gradients. They can move against the mean flow velocity (ie Morrison 1973) as in a stagnation flow or significantly faster than the mean flow velocity as in a nozzle flow. While these effects are not likely to be important in the far wake they could be significant in the development of the initial distribution. The axial and transverse pressure gradients can be large in the near wake where propeller swirl and over-thrust and ship drag velocities are large.

Summary and Conclusions

A model predicting bubble behavior in a ship wake is presented. Qualitatively, the predictions look very reasonable. No quantitative data is currently available for both hydrodynamic and bubble initial conditions. A sensitivity analysis was performed which indicates that no primary mechanism of bubble transport dominates. Convective transport, turbulent dispersion, and gas diffusion all have a significant influence in the down stream bubble distribution. The the need for a better fundamental understanding of bubble dynamics was clearly demonstrated by the large influence of empirical inputs to the model.

Acknowledgments

This work was performed under the ONT ship wake detection program. The authors are indebted to Dr. S. E. Ramberg for his many helpful suggestions and comments.

REFERENCES

1. Baker, A.J., 1982, NASA Contractor Report 3645
2. Bezzabotnov, V.S., 1985, Izvestiya, Atmos. and Ocean. Phys., vol. 21, p. 77.
3. Blanchard, D.C. and Woodcock, A.H., 1957, Tellus, vol. 9, no. 145.
4. DeVantier, B.A., and Larock, B.E., 1983, J. Hydraul. Eng., ASCE, vol. 109, no. 12.
5. Fox, F.E. and Herzfeld, K.F. 1954, J. Acoust. Soc., vol. 26, p. 984.
6. Garrettson, G.A., 1973, J. Fluid Mech., vol. 59, part 1, p. 187.
7. Johnson, B.D. and Cooke, R.C., 1979, J. Geophys. Res., vol. 84, NC 7, p. 3761.
8. Kanwisher, J., 1963, Deep-Sea Res., vol. 10, p. 195.
9. Ling, S.C., and Pao, H.P., 1987, ASCE Engineering Mechanics Division Specialty Conference, Buffalo, N.Y.
10. Medwin, H., 1970, J. Geophys. Res., vol. 75, p. 599.
11. Miner, E.W., Griffin, O.M., and Skop, R.A., 1986, NRL MR 5756.
12. Morrison, F.A. Jr., 1974, Aerosol Sci., vol. 5, p.241.
13. Schmidt, R., 1972, "Acoustic Properties of Wakes", NUSC TR 4096.
14. Shulkin, M., 1968, J. Acoust. Soc. Am., vol. 44, p. 1152.
15. Shulkin, M., 1969, J. Acoust. Soc. Am., vol. 45, p. 1054.
16. Smith, R.W., Hyman, M.C., amd Uzes, C.A., 1986, NCSC TM, U4210-86-29-40U17.
17. Stewart, M.B., and Morrison, F.A. Jr., 1981, J. Appl. Mech., Trans. ASME. vol.48, p.224.
18. Stewart, M.B., and Morrison, F.A. Jr., 1981, J. Appl. Mech., Trans. ASME. vol.48., p.436.
19. Stewart, M.B., 1987, NRL MR 5955.
20. Sutcliff, W.H., Baylor, E.R. and Nenzel, D.W., 1963, Deep Sea Res., vol. 10, p. 233.